

Article

A Comprehensive Biophysical Description of Pairwise Epistasis throughout an Entire Protein Domain

C. Anders Olson,^{1,*} Nicholas C. Wu,¹ and Ren Sun^{1,*}

¹Department of Molecular and Medical Pharmacology,
University of California, Los Angeles, Los Angeles, CA
90095, USA

Summary

Background: Nonadditivity in fitness effects from two or more mutations, termed epistasis, can result in compensation of deleterious mutations or negation of beneficial mutations. Recent evidence shows the importance of epistasis in individual evolutionary pathways. However, an unresolved question in molecular evolution is how often and how significantly fitness effects change in alternative genetic backgrounds.

Results: To answer this question, we quantified the effects of all single mutations and double mutations between all positions in the IgG-binding domain of protein G (GB1). By observing the first two steps of all possible evolutionary pathways using this fitness profile, we were able to characterize the extent and magnitude of pairwise epistasis throughout an entire protein molecule. Furthermore, we developed a novel approach to quantitatively determine the effects of single mutations on structural stability ($\Delta\Delta G_U$). This enabled determination of the importance of stability effects in functional epistasis. **Conclusions:** Our results illustrate common biophysical mechanisms for occurrences of positive and negative epistasis. Our results show pervasive positive epistasis within a conformationally dynamic network of residues. The stability analysis shows that significant negative epistasis, which is more common than positive epistasis, mostly occurs between combinations of destabilizing mutations. Furthermore, we show that although significant positive epistasis is rare, many deleterious mutations are beneficial in at least one alternative mutational background. The distribution of conditionally beneficial mutations throughout the domain demonstrates that the functional portion of sequence space can be significantly expanded by epistasis.

Introduction

Epistasis, within and between genes, is thought to play an essential role in the ability for protein sequences to evolve through neutral drift or adaptation [1, 2]. While contingencies in fitness limit pathways of divergence, permissive mutations reveal “cryptically beneficial” substitutions [3] that increase the number of acceptable mutations [4]. Epistasis can be explained in physical terms by investigating the biochemical effects of mutations singly and in combination [5]. Examples include evolution of a switch in glucocorticoid receptor-ligand specificity [6], increased hemoglobin affinity to O₂ in high-altitude deer mice [7], and antibiotic resistance in a β -lactamase variant [8], which all rely on nonadditive combinations of mutations.

The importance of epistasis is evident for organisms such as influenza that accumulate mutations at a high rate and adapt rapidly in response to immunological and drug pressure [9, 10]. Gong et al. demonstrated how an evolutionary pathway in influenza nucleoprotein required permissive stabilizing mutations prior to gaining certain adaptive substitutions that alone disrupted protein structure [10]. Indeed, most mutations destabilize protein structures [11, 12], and directed evolution experiments show that a large fraction of mutations are deleterious for function [13]. It was recently shown that 63 of 168 mutations chosen from a homologous protein with the same function were deleterious when substituted alone and thus that epistatic interactions are necessary to preserve function [14].

Although these examples show that epistasis is essential in individual evolutionary pathways, they do not address whether combinations of mutational fitness effects are typically epistatic. How likely is it that a mutation has the same fitness in two different genotypes? Historically, protein engineering experiments have shown that the effects of mutations on protein function are typically energetically additive [15–18]. Furthermore, next-generation sequencing technology has enabled the analysis of very large numbers of mutational pairs in experimental evolution which also show that fitness effects are usually additive [19, 20]. Here, we sought to determine whether this observation of general pairwise additivity conflicts with the apparent pervasiveness of epistasis in light of mutational sensitivity [14]. By analyzing the first two steps of all possible evolutionary pathways, we can determine the frequency of pairwise energetic nonadditivity.

Such a comprehensive analysis is necessary in order to determine how often deleterious mutations can be compensated by at least one additional mutation and, likewise, how often neutral or beneficial mutations can be negated by an additional mutation. To do this, we characterized a comprehensive fitness map of single and double mutants within protein G domain B1 (GB1) that was highly correlated to binding affinity (K_A) to immunoglobulin G fragment crystallizable (IgGFC). GB1 is well characterized structurally and is a classical model protein for folding and stability studies [21–24]. Although small, GB1 is a stable, compact, and highly soluble protein with no disulfide bonds. The structure includes an α -helix packed against a four-stranded β sheet that are connected by four short loops. This extensive structural and mutagenic characterization of GB1 provided a substantial reference for validating our fitness map.

Furthermore, we were able to use the fitness map to accurately predict the effect of all nonlethal single mutations on structural stability ($\Delta\Delta G_U$). This was accomplished by identifying destabilized mutational backgrounds in which the binding data reflects a change in fraction folded upon addition of secondary mutations. Thus, our fitness map enabled us to identify common biophysical mechanisms of both negative and positive epistasis. For example, we show that exhaustion of the intrinsic stability reservoir, or threshold robustness [25–27], largely accounts for examples of significant negative epistasis. Stabilizing substitutions, which are rare, produce positive epistasis, although with a smaller magnitude compared to combinations of destabilizing mutations. We also

*Correspondence: aolson@mednet.ucla.edu (C.A.O.), rsun@mednet.ucla.edu (R.S.)

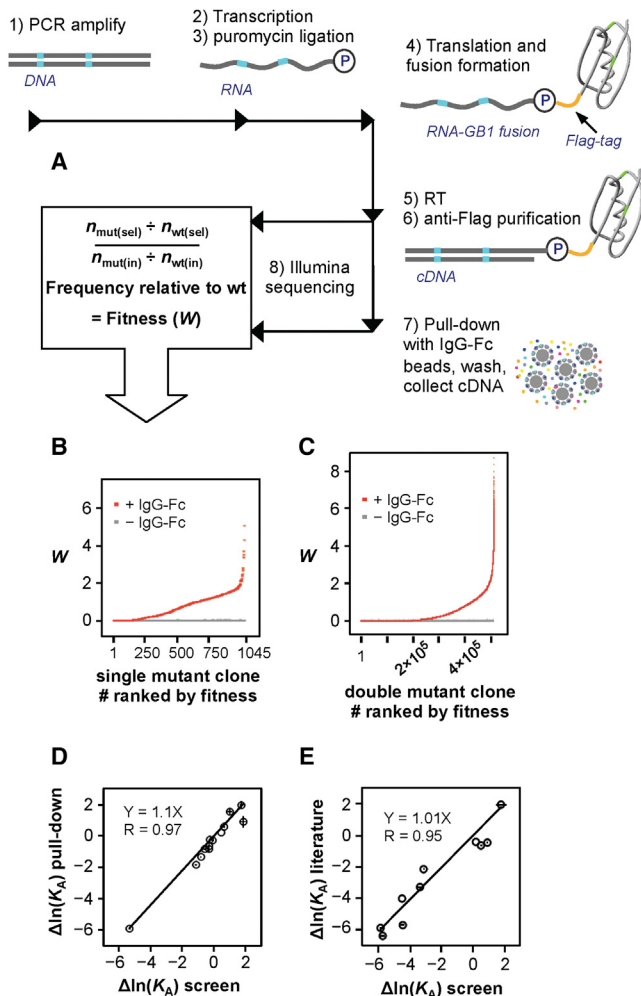


Figure 1. mRNA Display Fitness Profile Scheme

(A) A DNA library encoding all single and double mutants in GB1 was created (see also Figure S1). mRNA display was used to profile the relative binding efficiency of all variants. After a single generation of affinity enrichment, the relative fitness (W) for each variant was determined from the change in sequence frequency as identified by Illumina sequencing.

(B and C) The binding fitness (red dots) of each single mutant (B) and (C) all high-confidence double mutants (C; see Figure S1E). The gray dots represent the contribution to W from background binding to beads, which was determined from a control lacking IgG-FC.

(D) Thirteen clones were constructed and expressed in vitro with a 35 S-methionine label for comparison to fitness determined by the screen. Binding efficiency (see also Figure S1D) was used to estimate relative affinity (see the Experimental Procedures). Error bars represent SD from the triplicated screen (x axis) and from the pull-down when performed in triplicate (y axis).

(E) Correlation of $\Delta\ln(K_d)$ from the screen to $\Delta\ln(K_d)$ for ten variants reported in the literature (see Table S3).

See also Figure S1 and Table S1.

describe long-range positive epistasis that is pervasive within a highly conformationally dynamic network of residues. Our results confirm that epistasis is rare and also that many mutations are detrimental to function. However, this comprehensive fitness profile shows that many deleterious mutations are compensable by at least one of the numerous possible secondary mutations. Together, these results provide an empirical, biophysical description of epistasis and resolve how rare nonadditivity can contribute to the extensive divergence of protein sequences as observed in nature.

Results

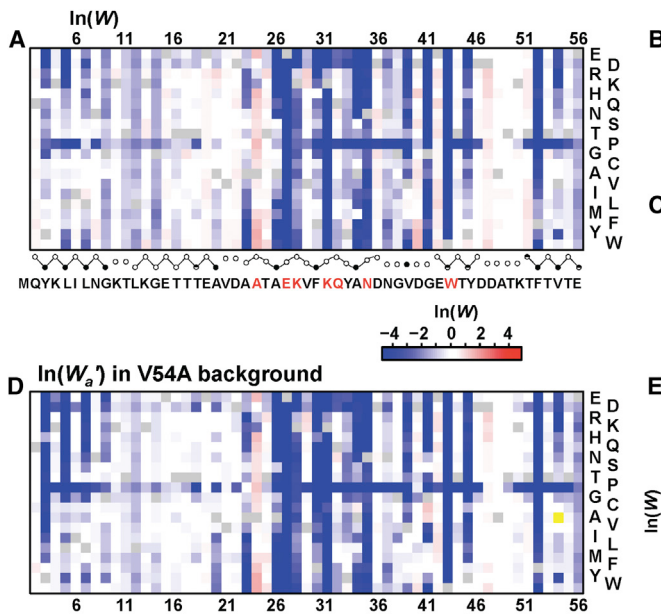
High-Resolution GB1 Double-Mutant Affinity Profile

We developed a cassette saturation-mutagenic approach for assembling a library that includes all single and double mutations within the 56 residue GB1 domain (excluding Met1) (Figure 1; Figure S1 and Table S1 available online). Two technical hurdles were overcome in this study: the ability to error correct and the ability to build a library that is focused on one or two amino acid mutations throughout the entire 55 codon random region. To enable sequencing error correction, we included internal barcodes in each cassette (Figure S1A). Linking of saturation-mutagenized cassettes was accomplished in a sequence-independent manner by using a type IIS restriction endonuclease (BbvI) (Figure S1B). After digestion, a single, degenerate M (A/C) overhang on 3' fragments enabled specific ligation to a G, T, or K (G/T) overhang on 5' fragments.

The use of in vitro display technologies to analyze the effects of individual mutations on binding function is well established [28, 29]. Next-generation sequencing has greatly expanded the ability to analyze mutational fitness effects quantitatively [30]. In this study, relative binding affinity of all single and nearly all double amino acid mutants to IgG-FC was characterized using mRNA display [31]. mRNA display is an in vitro genetic system in which peptides are covalently linked to the encoding mRNAs (Figure 1A) typically used to evolve novel molecular recognition tools [31, 32]. Here, we used deep sequencing combined with mRNA display to monitor the evolution of GB1 mutants in real time after one generation of affinity enrichment (Figure 1A).

By measuring the frequency of each variant before and after enrichment (Table S2), we determined relative binding efficiency, or fitness (Figures 1B, 1C, and S1D; see the Experimental Procedures). While fitness is traditionally a population-genetics term, protein fitness can be defined [30, 33, 34], and here relative fraction bound is analogous to a classical definition of relative fitness (W), which is the number of progeny relative to the wild-type (WT) per generation. The conditions of this screen, in which the concentration of IgG-FC is below the K_D of WT GB1, provided a large dynamic range in observed fitness effects, from 100-fold below to 8-fold higher than WT fitness (Figures 1B and 1C). Thus, our evolution experiment investigates affinity-based adaptation for improved or new function. We caution that this extremely simplified, noncompetitive evolutionary experiment has many differences in comparison to natural evolution and the relationship between affinity and in vivo fitness will not be directly correlated for many proteins, especially considering that many proteins are multifunctional. However, there are examples in natural evolution such as viral host switching that show a relationship between the affinity of host-adapted receptor binding domain variants and viral infectivity in cell culture [35].

Using a Poisson-based 90% confidence interval, we determined that the fitness effects of all 1,045 single mutants were determined with high confidence and 509,693 double mutants (95.1% of all) were characterized with high confidence (Figure S1E). Importantly, the high-confidence data set includes abundant double mutants throughout all 1,485 possible positional pairs (Figure S1E). The single generation of affinity enrichment was performed in triplicate, and Figure S1F shows that the single-mutant fitness profiles are highly correlated ($R > 0.996$ for all three comparisons). Thus, the binding, PCR, Illumina adaptor ligation, and sequencing steps are highly reproducible. Furthermore, we included a no-IgG control to



show that background binding does not affect fitness calculations for any variant, including mutants known to be unfolded (Figures 1B and 1C).

We also show that W can be used to approximate relative affinity ($K_{A\text{-mut}} / K_{A\text{-wt}}$) similar to the “shotgun scanning” approach [29] (see the [Experimental Procedures](#)). This was used to facilitate validation and enable the comparison of energetic effects to fitness effects. We show that $\Delta \ln(K_A)$ values predicted by this screen are highly correlated to those of 13 single or double mutants reconstructed and analyzed for validation by an *in vitro* pull-down assay (Figure 1D). Furthermore, the $\Delta \ln(K_A)$ predicted by the screen is highly correlated to that of an additional ten variants independently reported in the literature (Figure 1E and [Table S3](#)).

Figure 2A depicts $\ln(W)$ as a heatmap for all 19 single mutants at each position. The average $\ln(W)$ values per position are displayed on GB1 structures alone or in complex with IgG-FC (Figures 2B and 2C). As expected, core residues are sensitive to substitution [37], indicating severe structural destabilization or that small changes in structure that accommodate core volume changes might adversely affect binding affinity [38, 39]. Surface residues that are sensitive to mutation correlate with alanine scanning mutagenesis [40] and clarify relative importance for ligand recognition [21]. However, beneficial and detrimental surface mutations are found throughout the domain, thus highlighting the importance of such comprehensive screens for characterizing the sequence determinants of functionality [28, 30, 41–44]. For example, alanine scanning could not uncover the importance of position Thr25, where acidic substitutions are highly deleterious and basic substitutions are highly beneficial while Ala is neutral [40] (Figures 1E and 2A).

The double-mutant fitness landscape is depicted as a heatmap showing all high-confidence double mutants (up to 361) for all 1,485 positional pairs (Figure S2A). The comprehensive nature of this screen enables an alternative approach to interpret this data by showing the fitness of all substitutions (a) in alternative mutational backgrounds (b). For example, we show the fitness effects of all single mutants (W_a') in the

Figure 2. Affinity Profile Validation and Fitness Maps

(A) A heatmap depicting fitness of all single mutants. Residues previously determined to interact with IgG-FC [21] are highlighted in red. The fraction side-chain solvent accessibilities (closed circles, <0.1; partial circles, >0.1; open circles, >0.4) are depicted below. Circles are connected by straight or curved lines to delineate β strands and the α helix, respectively.

(B and C) Average $\ln(W)$ plotted on GB1 (PDB ID: 1PGA; B) [36] and the complex between protein G domain C2 (space filled) and IgG-FC (cartoon) (PDB ID: 1FCC; C) [21].

(D) A heatmap depicting fitness of all single mutants in the background of V54A.

(E) Comparison of the fitness profile to fitness effects in the background of V54A. See also [Figure S2](#).

background of V54A (Figures 2D and 2E). V54A alone is functionally neutral; however, certain positions become more sensitive to mutations, whereas others change from deleterious to

beneficial, notably at position Gly 41 (Figure 2D; *vide infra*). Furthermore, we show how the fitness of all mutations will change in the background of highly adaptive mutations, such as A24E, which is observed in nature (Figures S2B–S2D). In this background, the functional test is less stringent (i.e., the K_D of A24E is closer to $[IgG]$), and thus the distribution of fitness effects (DFE) [45] shifts significantly (Figures S2E–S2G), as it would in a less stringent test of fitness (Figure S2H).

Frequency and Proximity of Epistatic Interactions

Figures 2D and 2E show that certain mutations display a change in fitness in combination with V54A and are thus epistatic. Various models can be used to determine whether combinations of mutations display epistasis (ε) [19, 46, 47]. The difference between the fitness in Figure 2D and the fitness in Figure 2A produces one measure of epistasis [$\varepsilon = \ln(W_a') - \ln(W_a)$], which is identical to the relative epistasis model described by Kahn et al. [$\varepsilon = \ln(W_{ab}) - \ln(W_a) - \ln(W_b)$] [46]. We show that the relative model is suitable for the highly adaptive landscape of this experiment (Figure S3A). Here, epistasis (ε) refers to the relative model unless stated otherwise.

We displayed ε for all observed double mutants (Figure 3A) and the average ε for all substitutions at each pairwise positional combination (Figure 3B) as a heatmap. In addition to the 509,693 high-confidence variants, 7,585 variants were unambiguous in sign or significance in ε , resulting in characterization of 96.5% of all pairs. The 90% confidence interval (see above and the [Experimental Procedures](#)) was used to minimize epistasis resulting from very low-fitness double-mutants, which could display very large fold change in observed compared to expected fitness due to statistical noise. All 1,485 pairwise positional combinations are represented (Figure S1E), thereby providing a comprehensive description of epistasis throughout the entire protein molecule.

Generally, mutational pairs interact additively or nearly additively, and thus strongly epistatic pairs are rare (Figures 3C and S3B–S3G). This observation is in agreement with two recent large-scale analyses of epistasis [19, 20]. It is worth noting that although only a fraction of all double mutants display

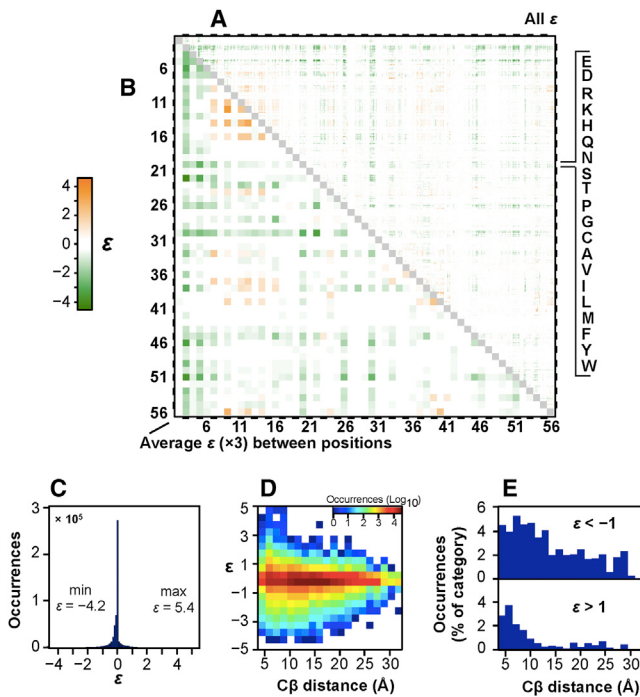


Figure 3. Pairwise Epistasis Map throughout GB1

(A) A heatmap depicting epistasis for 517,278 double mutants (96.5% of all possible). The amino acid order is listed top to bottom and is the same left to right. Each of the 1,485 pairs display 19×19 sequence variants.
 (B) Average ϵ for all sequence combinations at each positional combination multiplied by a factor of 3 in order to match the range of the color bar.
 (C) Histogram showing extent of epistasis (increments of 0.1).
 (D) 2D histogram relating ϵ to $C\beta$ distances in 1PGA [36].
 (E) $|\epsilon| > 1$ as a percentage of total occurrences in each $C\beta$ distance bin.
 See also Figure S3.

$|\epsilon| > 1$ (~4%), there are nonetheless thousands of such epistatic pairs (Figures S3B and S3C). We also show that epistasis is similarly rare when calculated using another common epistasis model, the product model (Figures S3E and S3F) [19]. Importantly, due to the low frequency or small magnitude of epistatic effects, the observed double-mutant DFE is nearly identical to the expected distribution (Figures S3H–S3L). Although lethal double mutants are slightly more frequent than would be predicted based on a model without epistasis (Figure S3H), this demonstrates the predictability of the distribution of multiple mutant fitness effects in this adaptive landscape. We also show that observed relative epistasis in this experiment closely matches a model of energetic nonadditivity (scaled by $-1/RT$; Figures S3M and S3N) [18]. The differences resulting from the nonlinear nature of the relationship between fraction bound and affinity are numerous but relatively small (Figure S3M). This would not be observed in a test of mutational robustness for well-adapted proteins, as is depicted by the DFE in Figure S2H.

As expected, strongly epistatic pairs tend to be close in space, although very large negative epistasis ($\epsilon < -3$) can be long range (Figure 3D). However, most neighboring residues do not display either form of epistasis (Figure 3E). Even considering interactions within 6 Å ($C\beta$), only 8.1% display $|\epsilon| > 1$. Thus, for many mutations, binding fitness is independent of the background in which one appears. For positions that are energetically coupled, double mutants might be predicted to

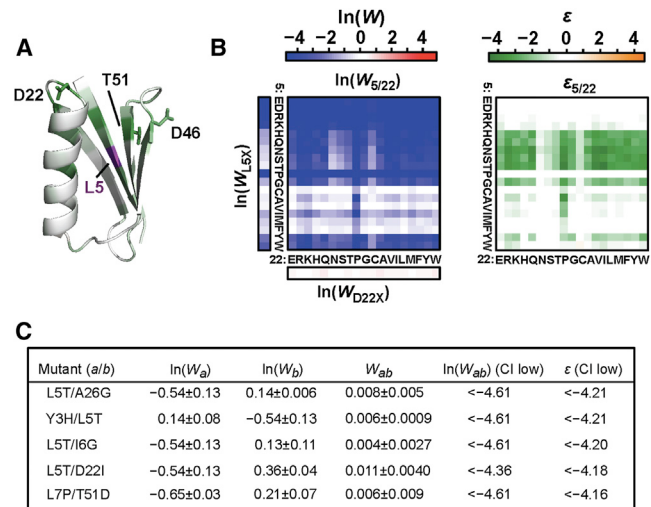


Figure 4. Positions Display Negative Epistasis in General Independent of Amino Acid Combination

(A) Average ϵ between position 5 and all other positions in GB1 (1PGA) [36]. Distant surface residues that demonstrate negative epistasis are labeled.
 (B) Binding fitness and epistasis for all 361 combinations of substitutions for Leu5 and Asp22. Leu5 is a critical core residue that is sensitive to mutation, whereas Asp22 is part of a helical capping motif near the binding surface, where substitutions are generally well tolerated for binding function.
 (C) The most significant values of negative epistasis are listed. Each pair includes mutations that are expected to destabilize the structure but alone do not unfold the protein or significantly disrupt affinity. A Poisson-based 90% confidence interval was used to generate an upper boundary for binding fitness, thereby enabling a conservative estimate of epistasis.
 See also Figure S4.

display either negative or positive epistasis depending on the physicochemical nature of the two amino acid substitutions. To highlight an example, the maps showing $\ln(W)$ and ϵ for all 361 amino acid combinations at positions 32 and 36 are enlarged (Figures S3O and S3P). However, an interesting observation from Figures 3A and 3B is that some positional combinations, including long-range combinations, display either negative or positive epistasis in general.

General Negative Epistasis throughout GB1

We wanted to determine what mechanism could explain general patterns of epistasis independent of specific amino acid identities. For example, core mutations, such as those at position 5 (Leu), display general negative epistasis with other positions throughout the domain (Figures 3B and 4A). In addition to general negative epistasis between substitutions at position 5 and other core positions, long-distance negative epistasis occurs between position 5 and surface positions within the stable $\beta_3\beta_4$ loop [22, 48], as well as substitutions for Asp22, a helical capping residue (Figure 4A). Figure 4B highlights $\ln(W)$ and ϵ for all 361 amino acid combinations within positions 5 and 22. The threshold robustness model [25–27] (Figures S4A–S4C) may explain the pervasive negative epistasis exhibited between these and similar residues. Most proteins are marginally stable [11, 12] yet withstand destabilizing mutations that do not significantly decrease the fraction of folded protein. However, when two such destabilizing substitutions combine, the stability “reservoir” can be exhausted thus resulting in a decrease in the fraction of

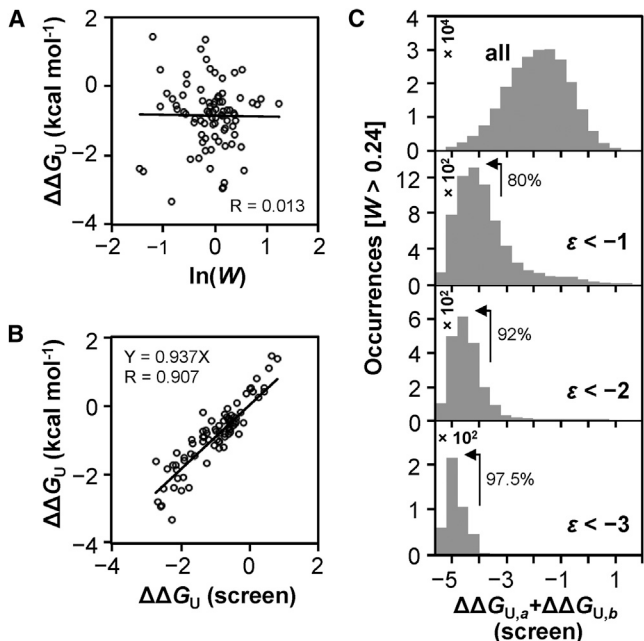


Figure 5. Relationship between Structural Stability Effects and Epistasis
(A) Comparison of $\ln(W)$ to free energy of unfolding relative to the WT ($\Delta\Delta G_U$) reported in the literature.
(B) The predicted thermodynamic stability of 82 single mutants compared to $\Delta\Delta G_U$ values reported in the literature (see Table S4). $\Delta\Delta G_U$ predicted by the screen are median values identified by estimating the change in fraction of unfolded protein in five destabilized mutant backgrounds. This analysis was limited to variants displaying $W > 0.24$ (709 of 1,045), as lower fitness values did not produce sufficient dynamic range to measure decreased structural stability.
(C) Histograms of $\Delta\Delta G_{U,a} + \Delta\Delta G_{U,b}$ showing how the distribution of predicted stability changes as the magnitude of negative epistasis increases. The percentage of each epistasis category resulting from combinations of significantly destabilized mutations (left of the arrow) is listed.
See also Figure S5 and Table S4.

native protein and a concomitant loss in function (Figures S4A–S4C). Thus, additive stability effects produce nonadditive functional effects. This model is consistent with the observation that large values of negative epistasis can be long range (Figures 3D and 3E). The threshold robustness model is also consistent with the observation that the combination of buried polar residues at position 5 and substitutions at 22 that abolish a helical capping motif display some of the largest values of negative epistasis observed (Figures 4C and S4D).

Structural Stability and Functional Epistasis

We further examined to what extent structural effects could account for examples of either negative or positive epistasis. To do this, we developed a method to estimate change in free energy of unfolding ($\Delta\Delta G_U$) for single mutants from the binding data. We found that $\ln(W)$ is uncorrelated to $\Delta\Delta G_U$ reported in the literature as expected for destabilizing mutations that remain folded at the screen temperature (Figures 5A and S4A and Table S4). However, for partially unfolded mutants, addition of a second mutation will increase the fraction unfolded (f_U) if destabilizing and, conversely, will increase the native fraction (f_N) if stabilizing. As noted above, the threshold robustness effect can be explained as additive stability effects that produce nonadditive functional effects (Figure S4). We

hypothesized that certain mutants might be identified that satisfy the condition $W_a = f_{N,a}$, and if these backgrounds are generally noninteracting other than through stability effects, we can estimate $f_{N,ab} = W_{ab} / W_b$. The predicted $f_{N,ab}$ can then be used to estimate structural stability of single mutants (b) by $\Delta\Delta G_U = -RT \times \ln(f_{U,ab} / f_{N,ab}) + RT \times \ln(f_{U,a} / f_{N,a})$.

The large number of GB1 variants characterized in the literature provided a substantial reference to identify stability effects from the binding data. An automated analysis was performed that identified multiple background mutations (a) that generated $\Delta\Delta G_U$ values that correlate well with the values found in the literature. These backgrounds therefore satisfy the conditions stated above. This method is limited however to mutants (b) with sufficient fitness to produce a dynamic range in observed fitness (ab; those with $W_b < 0.24$ correlated poorly). An average of the values generated from five reference backgrounds (Y3A, Y3C, L5N, L5S, and F30N) was highly correlated to 82 $\Delta\Delta G_U$ values published in the literature with a slope of 0.94 and a correlation coefficient (R) of 0.907. We note that this correlation is very good considering variability in experimental $\Delta\Delta G_U$ calculations illustrated by Potapov et al. [49]. They show that the correlation (R) between 406 pairs of $\Delta\Delta G_U$ values reported for identical protein variants is 0.86.

In order to estimate the importance of the threshold robustness effect in shaping the GB1 double-mutant fitness landscape, we estimated the structural stability of double mutants by summing $\Delta\Delta G_U$ and determined the number of occurrences of significant negative epistasis for different predicted double mutant stabilities (Figure 5C). For some combinations, $\Delta\Delta G_U$ will not be additive (Figures S5A–S5C and Table S5), which can mitigate the threshold robustness effect. However, as negative epistasis becomes more significant, double mutants predicted to be very unstable account for most occurrences (Figure 5C). For example, 97.5% of all double mutants displaying $\epsilon < -3$ are predicted to be at least 4 kcal mol⁻¹ less stable than WT GB1. Thus, our study empirically demonstrates the extent of the threshold robustness model in functional epistasis.

It is also expected that positive epistasis will arise from stability effects. This will occur if a stabilizing mutation increases the fraction of native protein in the background of a highly destabilized mutant that is partially unfolded at room temperature. Stabilizing mutations have been shown to set the stage for evolution by permitting adaptive mutations that are destabilizing alone [10, 50, 51]. However, it is known that stabilizing mutations are lower in frequency and in magnitude compared to destabilizing mutations [12], and this is corroborated by our screen (Figure S5D). Thus, additive effects from the smaller number and magnitudes of stabilizing mutations overall contribute less to epistasis in comparison with additive effects from combinations of two destabilizing substitutions (Figures S5E–S5J).

General Positive Epistasis within a Dynamic Region

In addition to general negative epistasis, it is also apparent that combinations of mutations within a smaller group of positions display positive epistasis on average (Figure 3B). One position is A24, which shows that positive epistasis is correlated with low-fitness positions and negative epistasis is correlated with high-fitness positions (Figure S6A; see also Figures S2C and S2D). Other positions that display positive epistasis in general include residues within the β 1- β 2 loop (7, 9, 11), β strand 2 (12, 14, 16), C-terminal end of the α helix through the α - β 3 loop (33, 37, 38, 40), and C-terminal β 4 residues

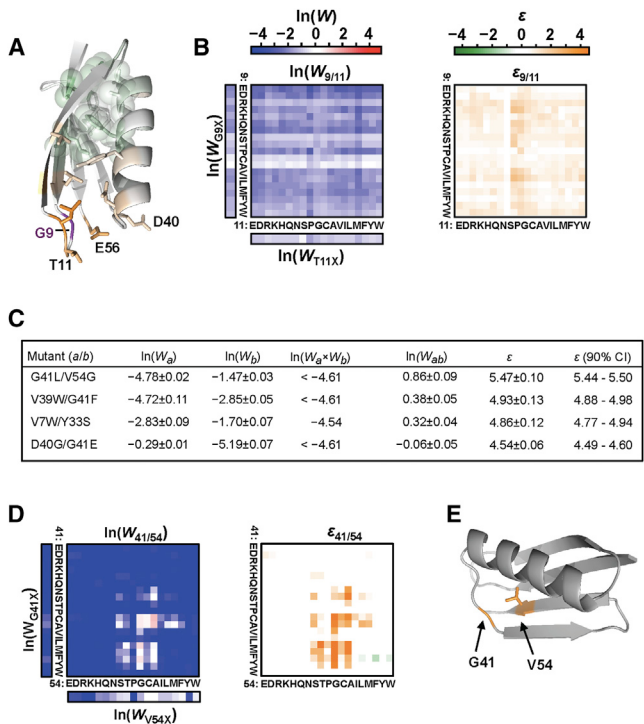


Figure 6. Positions that Display General Positive Epistasis Independent of Amino Acid Combination

(A) Average ε for all pairwise combinations with position 9. Glu56, which couples the two dynamic loops through H bonds, is highlighted.
 (B) Epistasis and binding fitness for all 361 combinations of substitutions for G9 and T11, which are located within the highly dynamic β 1- β 2 loop.
 (C) The 20 most significant examples of positive epistasis include double mutants from four pairwise positional combinations. The double mutants displaying the largest value of positive epistasis per positional pair are listed. These combinations include neighboring residues within or at the edge of the conformationally dynamic region that overall demonstrates pervasive positive epistasis (see Figures 3A and 3B). For calculating epistasis, we limited expected fitness by $\ln(W_a \times W_b) \geq \ln(0.01)$ to minimize spurious epistasis values for lethal or nearly lethal double mutants resulting from nonmeaningful predicted fitness values below the background ($\sim W = 0.01$).
 (D) Fitness and epistasis for all double mutants including positions 41 and 54.
 (E) Exchanging volume from core residue Val54 to Gly41 demonstrates the most extreme value of positive epistasis.

See also Figure S6.

(54, 56) (Figures 3B and S6B–S6D). These residues participate in a network of residues that undergo correlated conformational dynamics [52–54]. Remarkably, the pattern of general positive epistasis seen in Figure 3B is very similar to that of correlated NH bond vector motions modeled by Lange et al. [54].

Combinations of mutations within the 12 positions listed in the dynamic region account for 49% of epistasis values >1 , while accounting for only 4.4% of all pairs. Figure 6A shows the structure of GB1 depicting the average epistasis between substitutions for Gly9 and mutations at all other positions. This region directly contacts IgG-FC through a main-chain H bond between the Val39 carbonyl oxygen and Asn434 on IgG [21]. This loop is coupled to the β 1- β 2 loop through H bonds between the C-terminal Glu56 carboxylate with the Asp40 and Lys10 amides [36] (Figure 6A). The dynamic region extends through β strand 2, which is located on the opposite side of

GB1 relative to the IgG-FC binding surface. Note that several mutations within this dynamic region also display slightly negative epistasis on average with substitutions in the protein core (Figures 3B and 6A). This is consistent with the threshold robustness effect as such substitutions are predicted to decrease the stability of the structure.

Many of the residues in the coupled, dynamic region of GB1 are generally sensitive to substitution (Figure 2C). For example, all 361 possible combinations of substitutions for G9 and T11 are highlighted (Figure 6B). The data show that when one mutation reduces fitness, an additional mutation in this region imparts a diminished negative effect. We constructed G9A, T11A, and the double mutant G9A/T11A to validate this epistatic effect (Figure S3A). This validation also confirms that subtle changes in amino acid identity in this region can have a significant effect on binding fitness from a distance (Figures 2A and 2C).

In some cases, combinations of substitutions in the dynamic region result in dramatic reversal of lethal fitness to positive fitness (Figure 6C). The most extreme example, G41L/V54G, results in the exchange of volume from the C-terminal core residue Val54 to the α - β 3 loop (Figures 6D and 6E). However, how the loop conformation can change to accommodate this swap is not intuitive either by manual inspection or through computational analysis using the parameters described by Kellogg et al. [55]. Interestingly, a highly diverged homolog of protein G of identical length demonstrates the sequence variation 41L/54G (Figure S6E). Furthermore, analysis by EVfold shows that this is a highly coevolving pair [56]. In summary, this analysis has uncovered an important role for residues involved in a dynamic network in contributing to GB1 function and identified how nonadditivity in this region, in some cases extreme, affects the double mutant fitness landscape.

Impact of Epistasis on Adaptive Pathways

While context independent fitness effects generally dominate the mutational landscape of GB1 (Figures 3C–3E), epistasis may promote or limit mutational walks in sequence space (Figure S7A). While most pairs do not display large positive epistasis, there are 37,405 pairs (7.2%) that display $\varepsilon > 0.15$. We wanted to determine how positive epistatic effects are distributed throughout the domain. We calculated fitness for each single mutant in all alternative backgrounds [$\ln(W'_a) = \ln(W_{ab}) - \ln(W_b)$] and show the range between the highest [if $\ln(W_{ab}) > -2$] and lowest values in comparison to the fitness in the WT background (Figure 7A). Many deleterious mutations display significantly improved fitness in at least one of the 1,026 possible non-WT backgrounds. In fact, of the 678 single mutations that are deleterious in the WT background, the fitness of 429 can reverse in sign [$\ln(W'_a) > 0$] and are thus compensable. Even considering only beneficial double mutants [$\ln(W_{ab}) > 0$], more than one-third of the deleterious mutations (240 of 678) reverse in sign in at least one alternative mutational background and are therefore “cryptically beneficial” (Figures 7B and S7C).

Discussion

With next-generation sequencing, the number of sequence variants in highly diverse populations can be counted before and after laboratory-designed tests of fitness, thereby quantifying evolution [30, 34, 41–44, 57–60]. An important question related to such studies is how often the observed fitness effects would change in the background of other mutations.

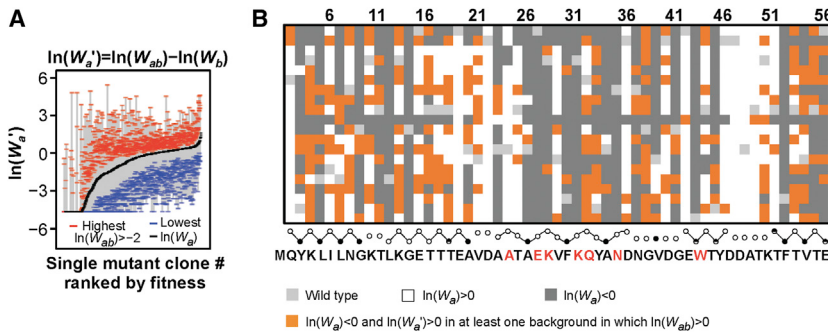


Figure 7. The Fitness Effects of Many Mutations Change Dramatically Depending on the Background in which They Appear

(A) The range is bound by a blue dash for the lowest fitness in any of the 1,026 possible alternate backgrounds and by a red dash for the highest fitness. The highest fitness values are limited to double mutants displaying $\ln(W_{ab}) > -2$.
(B) A map showing deleterious single mutants that are beneficial in at least one alternative mutational background even while limiting double-mutant fitness greater than the WT (orange). See also Figure S7.

Fields and colleagues have demonstrated the ability to characterize thousands of single and double mutants in segments of protein domains and thus make important conclusions on the frequency and nature of epistasis in protein function [19, 20]. In this article, we observe the first two steps of all evolutionary pathways in the recognition of IgG by GB1 and therefore observe how fitness profiles change in all alternative mutational backgrounds. This comprehensive analysis determines how often deleterious effects are compensated and beneficial effects are negated for all mutations in an entire protein molecule.

The fitness profile in Figure 1B and the DFE in Figure S2E show that the stringency of this fitness challenge is analogous to evolution of new function. It is well understood that the highest affinity possible will often not be selected for function in vivo [28]. However, the beneficial mutations we identify in vitro are found in natural protein G homologs (Figure S2B), and one homolog that does not benefit from tandem duplication has seven mutations that are all adaptive in this screen (see Figure S2B). Furthermore, there are ligand pairs that demonstrate a functional demand for exceptional affinity [61], including for IgG binding proteins similar to GB1 [62]. Such an adaptive landscape as described in this experiment could possibly be analogous to natural evolution in viral receptor host switching. For example, mutations found after adaptation of SARS from civet to human show enhanced affinity to receptor in vitro, and those mutations enhanced viral infectivity in cell culture [35]. Furthermore, affinity-based adaptation can occur if ligand concentrations decrease, for example, as observed in increased affinity for O₂ in high-altitude deer mouse hemoglobin [7].

We show common biophysical mechanisms for both negative and positive epistasis, including how additive stability effects produce functional epistasis. Although the environment of the cell will modulate the concentration of functional protein compared to what is observed in vitro [63], there is a clear relationship between protein stability and fitness in cells and viruses [10, 27, 64]. The cooperative nature of protein folding creates an inherently epistatic effect from additive stability effects [25–27]. In this experiment, additive effects of destabilizing mutations account for nearly all examples of very large negative epistasis. That destabilizing mutations are both more common and larger in magnitude compared to stabilizing mutations [12] explains why there are more significant negative epistatic effects compared to positive epistatic effects in this experiment. Stabilizing mutations might display stronger epistatic effects in vivo, however, by counteracting degradation or aggregation, such as been demonstrated in β-lactamase evolution [8].

Furthermore, we demonstrated that long-range deleterious fitness effects throughout a dynamic region are not additive

and therefore that mutations in this region display positive epistasis in general. These observations mirror results from extensive characterization of PDZ domains, which also display long-range mutational sensitivity in dynamic regions [43, 65, 66]. This effect can be exploited for allosteric modulation in nature or through engineering [67, 68]. The most substantial occurrences of positive epistasis were found in the region between positions in which two highly deleterious mutations combine to produce neutral or beneficial double mutants. A similar “hot spot” of epistasis predicted to produce a conformational switch that removes unfavorable interactions was also seen in an exceptionally high-throughput mutagenic study of an RRM domain [20].

The results of this paper reconcile observations about the importance of epistasis in adaptive evolution despite the rarity of it. We can see that while it should not be expected that mutations have different fitness in alternative backgrounds, most mutations can have a very different effect in at least one alternative genetic background. Cryptically beneficial mutations [$\ln(W_a') > 0$ and $\ln(W_{ab}) > 0$] are found throughout 43 positions in the 55-residue domain. Furthermore, while the WT is optimal at 17 positions, compensatory mutations reveal beneficial mutations within ten of these 17 positions even when limiting $\ln(W_{ab}) > 0$. Thus, while sign epistasis limits pathways of adaptation, it at the same time facilitates sequence change in light of mutational sensitivity.

Experimental Procedures

See the [Supplemental Experimental Procedures](#) for complete details for library construction, mRNA display and affinity enrichment, sequencing, data analysis, and validation.

Calculation of Structural Stability Effects

In order to estimate change in fraction folded, we assumed there will be mutational backgrounds (a) in which $W_{ab} / W_b = f_{N,ab}$. This can occur if the reference mutations are partially folded but neutral in the native state, if the test mutant (b) is fully folded in the native state, and if the two mutations do not interact functionally (only through additive thermodynamic stability effects). Thus, these conditions mean, given that the observed W is a product of the fraction folded and fitness of the native state ($W = f_N \times W_N$), that the background mutations must satisfy $f_{N,a} = W_a / W_{N,a} = 1$ and the test mutants (b) must satisfy $f_{N,b} = 1$. Therefore, for pairs that are energetically additive, $W_{N,ab} = W_b$. Substituting into $W_{ab} = f_{N,ab} \times W_{N,ab}$ gives us $f_{N,ab} = W_{ab} / W_b$. We automatically converted the 82 test mutants from the literature (Table S4) into $f_{N,ab}$ using all suitable backgrounds ($0 < W_a < 1$) and then into relative free energy of unfolding. At equilibrium, $k_F \times [U] = k_{Un} \times [N]$, and thus $f_{U,ab} / f_{N,ab} = k_{Un} / k_F$, which by definition equals K_{Un} and therefore $\Delta\Delta G_U = -RT \times \ln(f_{U,ab} / f_{N,ab}) + RT \times \ln(f_{U,a} / f_{N,a})$. Numerous substitutions at positions Y3, L15, F30, and A26 produced highly correlated data. The average $\Delta\Delta G_U$ values from the top five backgrounds from positions 3, 5, and 30 (Y3A, Y3C, L5N, L5S, and F30N) produced highly correlated data with a slope close to 1.

Supplemental Information

Supplemental Information includes Supplemental Experimental Procedures, seven figures, and five tables and can be found with this article online at <http://dx.doi.org/10.1016/j.cub.2014.09.072>.

Author Contributions

C.A.O. designed the experiments, performed the experiments, analyzed the data, and wrote the manuscript. N.C.W. created all scripts, analyzed the data, and revised the manuscript. R.S. designed experiments, provided intellectual support, and revised the manuscript.

Acknowledgments

R.S. was supported by the NIH (R21AI110261 and R01AI085583). C.A.O. was supported by NCI Cancer Education Grant R25 CA 098010. N.C.W. was supported by a UCLA MBI Whitcome grant. We thank X. Li for technical advice. We thank T.T. Wu, L.Q. Al-Mawsawi, T.T. Takahashi, R.W. Roberts, and J. Lloyd-Smith for comments.

Received: June 5, 2014

Revised: August 6, 2014

Accepted: September 25, 2014

Published: October 16, 2014

References

1. Breen, M.S., Kemeza, C., Vlasov, P.K., Notredame, C., and Kondrashov, F.A. (2012). Epistasis as the primary factor in molecular evolution. *Nature* **490**, 535–538.
2. Kimura, M. (1991). Recent development of the neutral theory viewed from the Wrightian tradition of theoretical population genetics. *Proc. Natl. Acad. Sci. USA* **88**, 5969–5973.
3. Weinreich, D.M., Watson, R.A., and Chao, L. (2005). Perspective: sign epistasis and genetic constraint on evolutionary trajectories. *Evolution* **59**, 1165–1174.
4. Povolotskaya, I.S., and Kondrashov, F.A. (2010). Sequence space and the ongoing expansion of the protein universe. *Nature* **465**, 922–926.
5. Harms, M.J., and Thornton, J.W. (2013). Evolutionary biochemistry: revealing the historical and physical causes of protein properties. *Nat. Rev. Genet.* **14**, 559–571.
6. Bridgman, J.T., Ortlund, E.A., and Thornton, J.W. (2009). An epistatic ratchet constrains the direction of glucocorticoid receptor evolution. *Nature* **461**, 515–519.
7. Natarajan, C., Inoguchi, N., Weber, R.E., Fago, A., Moriyama, H., and Storz, J.F. (2013). Epistasis among adaptive mutations in deer mouse hemoglobin. *Science* **340**, 1324–1327.
8. Weinreich, D.M., Delaney, N.F., Depristo, M.A., and Hartl, D.L. (2006). Darwinian evolution can follow only very few mutational paths to fitter proteins. *Science* **312**, 111–114.
9. Kryazhimskiy, S., Dushoff, J., Bazykin, G.A., and Plotkin, J.B. (2011). Prevalence of epistasis in the evolution of influenza A surface proteins. *PLoS Genet.* **7**, e1001301.
10. Gong, L.I., Suchard, M.A., and Bloom, J.D. (2013). Stability-mediated epistasis constrains the evolution of an influenza protein. *Elife* **2**, e00631.
11. Bloom, J.D., Raval, A., and Wilke, C.O. (2007). Thermodynamics of neutral protein evolution. *Genetics* **175**, 255–266.
12. Tokuriki, N., Stricher, F., Schymkowitz, J., Serrano, L., and Tawfik, D.S. (2007). The stability effects of protein mutations appear to be universally distributed. *J. Mol. Biol.* **369**, 1318–1332.
13. Romero, P.A., and Arnold, F.H. (2009). Exploring protein fitness landscapes by directed evolution. *Nat. Rev. Mol. Cell Biol.* **10**, 866–876.
14. Lunzer, M., Golding, G.B., and Dean, A.M. (2010). Pervasive cryptic epistasis in molecular evolution. *PLoS Genet.* **6**, e1001162.
15. Wells, J.A. (1990). Additivity of mutational effects in proteins. *Biochemistry* **29**, 8509–8517.
16. Sandberg, W.S., and Terwilliger, T.C. (1993). Engineering multiple properties of a protein by combinatorial mutagenesis. *Proc. Natl. Acad. Sci. USA* **90**, 8367–8371.
17. Gregoret, L.M., and Sauer, R.T. (1993). Additivity of mutant effects assessed by binomial mutagenesis. *Proc. Natl. Acad. Sci. USA* **90**, 4246–4250.
18. LiCata, V.J., and Ackers, G.K. (1995). Long-range, small magnitude nonadditivity of mutational effects in proteins. *Biochemistry* **34**, 3133–3139.
19. Araya, C.L., Fowler, D.M., Chen, W., Muniez, I., Kelly, J.W., and Fields, S. (2012). A fundamental protein property, thermodynamic stability, revealed solely from large-scale measurements of protein function. *Proc. Natl. Acad. Sci. USA* **109**, 16858–16863.
20. Melamed, D., Young, D.L., Gamble, C.E., Miller, C.R., and Fields, S. (2013). Deep mutational scanning of an RRM domain of the *Saccharomyces cerevisiae* poly(A)-binding protein. *RNA* **19**, 1537–1551.
21. Sauer-Eriksson, A.E., Kleywegt, G.J., Uhlén, M., and Jones, T.A. (1995). Crystal structure of the C2 fragment of streptococcal protein G in complex with the Fc domain of human IgG. *Structure* **3**, 265–278.
22. McCallister, E.L., Alm, E., and Baker, D. (2000). Critical role of beta-hairpin formation in protein G folding. *Nat. Struct. Biol.* **7**, 669–673.
23. Malakauskas, S.M., and Mayo, S.L. (1998). Design, structure and stability of a hyperthermophilic protein variant. *Nat. Struct. Biol.* **5**, 470–475.
24. Wunderlich, M., Max, K.E., Roske, Y., Mueller, U., Heinemann, U., and Schmid, F.X. (2007). Optimization of the gbeta1 domain by computational design and by *in vitro* evolution: structural and energetic basis of stabilization. *J. Mol. Biol.* **373**, 775–784.
25. Bloom, J.D., Silberg, J.J., Wilke, C.O., Drummond, D.A., Adam, C., and Arnold, F.H. (2005). Thermodynamic prediction of protein neutrality. *Proc. Natl. Acad. Sci. USA* **102**, 606–611.
26. Bershtein, S., Segal, M., Bekerman, R., Tokuriki, N., and Tawfik, D.S. (2006). Robustness-epistasis link shapes the fitness landscape of a randomly drifting protein. *Nature* **444**, 929–932.
27. Tokuriki, N., and Tawfik, D.S. (2009). Stability effects of mutations and protein evolvability. *Curr. Opin. Struct. Biol.* **19**, 596–604.
28. Pál, G., Kouadio, J.L., Artis, D.R., Kossiakoff, A.A., and Sidhu, S.S. (2006). Comprehensive and quantitative mapping of energy landscapes for protein-protein interactions by rapid combinatorial scanning. *J. Biol. Chem.* **281**, 22378–22385.
29. Weiss, G.A., Watanabe, C.K., Zhong, A., Goddard, A., and Sidhu, S.S. (2000). Rapid mapping of protein functional epitopes by combinatorial alanine scanning. *Proc. Natl. Acad. Sci. USA* **97**, 8950–8954.
30. Fowler, D.M., Araya, C.L., Fleishman, S.J., Kellogg, E.H., Stephany, J.J., Baker, D., and Fields, S. (2010). High-resolution mapping of protein sequence-function relationships. *Nat. Methods* **7**, 741–746.
31. Roberts, R.W., and Szostak, J.W. (1997). RNA-peptide fusions for the *in vitro* selection of peptides and proteins. *Proc. Natl. Acad. Sci. USA* **94**, 12297–12302.
32. Olson, C.A., Nie, J., Diep, J., Al-Shyukh, I., Takahashi, T.T., Al-Mawsawi, L.Q., Bolin, J.M., Elwell, A.L., Swanson, S., Stewart, R., et al. (2012). Single-round, multiplexed antibody mimetic design through mRNA display. *Angew. Chem. Int. Ed. Engl.* **51**, 12449–12453.
33. Soskine, M., and Tawfik, D.S. (2010). Mutational effects and the evolution of new protein functions. *Nat. Rev. Genet.* **11**, 572–582.
34. Firnberg, E., Labonte, J.W., Gray, J.J., and Ostermeier, M. (2014). A comprehensive, high-resolution map of a gene's fitness landscape. *Mol. Biol. Evol.* **31**, 1581–1592.
35. Wu, K., Peng, G., Wilken, M., Geraghty, R.J., and Li, F. (2012). Mechanisms of host receptor adaptation by severe acute respiratory syndrome coronavirus. *J. Biol. Chem.* **287**, 8904–8911.
36. Gallagher, T., Alexander, P., Bryan, P., and Gilliland, G.L. (1994). Two crystal structures of the B1 immunoglobulin-binding domain of streptococcal protein G and comparison with NMR. *Biochemistry* **33**, 4721–4729.
37. Lesk, A.M., and Chothia, C. (1980). How different amino acid sequences determine similar protein structures: the structure and evolutionary dynamics of the globins. *J. Mol. Biol.* **136**, 225–270.
38. Di Nardo, A.A., Larson, S.M., and Davidson, A.R. (2003). The relationship between conservation, thermodynamic stability, and function in the SH3 domain hydrophobic core. *J. Mol. Biol.* **333**, 641–655.
39. Xu, J., Baase, W.A., Baldwin, E., and Matthews, B.W. (1998). The response of T4 lysozyme to large-to-small substitutions within the core and its relation to the hydrophobic effect. *Protein Sci.* **7**, 158–177.
40. Sloan, D.J., and Hellinga, H.W. (1999). Dissection of the protein G B1 domain binding site for human IgG Fc fragment. *Protein Sci.* **8**, 1643–1648.
41. Wu, N.C., Young, A.P., Al-Mawsawi, L.Q., Olson, C.A., Feng, J., Qi, H., Chen, S.H., Lu, I.H., Lin, C.Y., Chin, R.G., et al. (2014). High-throughput profiling of influenza A virus hemagglutinin gene at single-nucleotide resolution. *Sci. Rep.* **4**, 4942.

42. Roscoe, B.P., Thayer, K.M., Zeldovich, K.B., Fushman, D., and Bolon, D.N. (2013). Analyses of the effects of all ubiquitin point mutants on yeast growth rate. *J. Mol. Biol.* **425**, 1363–1377.
43. McLaughlin, R.N., Jr., Poelwijk, F.J., Raman, A., Gosal, W.S., and Ranganathan, R. (2012). The spatial architecture of protein function and adaptation. *Nature* **491**, 138–142.
44. Qi, H., Olson, C.A., Wu, N.C., Ke, R., Loverdo, C., Chu, V., Truong, S., Remenyi, R., Chen, Z., Du, Y., et al. (2014). A quantitative high-resolution genetic profile rapidly identifies sequence determinants of hepatitis C viral fitness and drug sensitivity. *PLoS Pathog.* **10**, e1004064.
45. Eyre-Walker, A., and Keightley, P.D. (2007). The distribution of fitness effects of new mutations. *Nat. Rev. Genet.* **8**, 610–618.
46. Khan, A.I., Dinh, D.M., Schneider, D., Lenski, R.E., and Cooper, T.F. (2011). Negative epistasis between beneficial mutations in an evolving bacterial population. *Science* **332**, 1193–1196.
47. Mani, R., St Onge, R.P., Hartman, J.L., 4th, Giaever, G., and Roth, F.P. (2008). Defining genetic interaction. *Proc. Natl. Acad. Sci. USA* **105**, 3461–3466.
48. Blanco, F.J., Rivas, G., and Serrano, L. (1994). A short linear peptide that folds into a native stable beta-hairpin in aqueous solution. *Nat. Struct. Biol.* **1**, 584–590.
49. Potapov, V., Cohen, M., and Schreiber, G. (2009). Assessing computational methods for predicting protein stability upon mutation: good on average but not in the details. *Protein Eng. Des. Sel.* **22**, 553–560.
50. Bloom, J.D., Labthavikul, S.T., Otey, C.R., and Arnold, F.H. (2006). Protein stability promotes evolvability. *Proc. Natl. Acad. Sci. USA* **103**, 5869–5874.
51. Tokuriki, N., Stricher, F., Serrano, L., and Tawfik, D.S. (2008). How protein stability and new functions trade off. *PLoS Comput. Biol.* **4**, e1000002.
52. Markwick, P.R., Bouvignies, G., and Blackledge, M. (2007). Exploring multiple timescale motions in protein GB3 using accelerated molecular dynamics and NMR spectroscopy. *J. Am. Chem. Soc.* **129**, 4724–4730.
53. Clore, G.M., and Schwieters, C.D. (2004). Amplitudes of protein backbone dynamics and correlated motions in a small alpha/beta protein: correspondence of dipolar coupling and heteronuclear relaxation measurements. *Biochemistry* **43**, 10678–10691.
54. Lange, O.F., Grubmüller, H., and de Groot, B.L. (2005). Molecular dynamics simulations of protein G challenge NMR-derived correlated backbone motions. *Angew. Chem. Int. Ed. Engl.* **44**, 3394–3399.
55. Kellogg, E.H., Leaver-Fay, A., and Baker, D. (2011). Role of conformational sampling in computing mutation-induced changes in protein structure and stability. *Proteins* **79**, 830–838.
56. Marks, D.S., Colwell, L.J., Sheridan, R., Hopf, T.A., Pagnani, A., Zecchina, R., and Sander, C. (2011). Protein 3D structure computed from evolutionary sequence variation. *PLoS ONE* **6**, e28766.
57. Deng, Z., Huang, W., Bakkalbasi, E., Brown, N.G., Adamski, C.J., Rice, K., Muzny, D., Gibbs, R.A., and Palzkill, T. (2012). Deep sequencing of systematic combinatorial libraries reveals β -lactamase sequence constraints at high resolution. *J. Mol. Biol.* **424**, 150–167.
58. Thyagarajan, B., and Bloom, J.D. (2014). The inherent mutational tolerance and antigenic evolvability of influenza hemagglutinin. *Elife* **3**, e03300.
59. Traxlmayr, M.W., Hasenhindl, C., Hackl, M., Stadlmayr, G., Rybka, J.D., Borth, N., Grillari, J., Rüker, F., and Obinger, C. (2012). Construction of a stability landscape of the CH3 domain of human IgG1 by combining directed evolution with high throughput sequencing. *J. Mol. Biol.* **423**, 397–412.
60. Hietpas, R.T., Jensen, J.D., and Bolon, D.N. (2011). Experimental illumination of a fitness landscape. *Proc. Natl. Acad. Sci. USA* **108**, 7896–7901.
61. Schreiber, G., Buckle, A.M., and Fersht, A.R. (1994). Stability and function: two constraints in the evolution of barstar and other proteins. *Structure* **2**, 945–951.
62. Nitsche-Schmitz, D.P., Johansson, H.M., Sastalla, I., Reissmann, S., Frick, I.M., and Chhatwal, G.S. (2007). Group G streptococcal IgG binding molecules FOG and protein G have different impacts on opsonination by C1q. *J. Biol. Chem.* **282**, 17530–17536.
63. Hingorani, K.S., and Giersch, L.M. (2014). Comparing protein folding in vitro and in vivo: foldability meets the fitness challenge. *Curr. Opin. Struct. Biol.* **24**, 81–90.
64. Mayer, S., Rüdiger, S., Ang, H.C., Joerger, A.C., and Fersht, A.R. (2007). Correlation of levels of folded recombinant p53 in escherichia coli with thermodynamic stability in vitro. *J. Mol. Biol.* **372**, 268–276.
65. Gianni, S., Haq, S.R., Montemiglio, L.C., Jürgens, M.C., Engström, A., Chi, C.N., Brunori, M., and Jemth, P. (2011). Sequence-specific long range networks in PSD-95/discs large/ZO-1 (PDZ) domains tune their binding selectivity. *J. Biol. Chem.* **286**, 27167–27175.
66. Petit, C.M., Zhang, J., Sapienza, P.J., Fuentes, E.J., and Lee, A.L. (2009). Hidden dynamic allostery in a PDZ domain. *Proc. Natl. Acad. Sci. USA* **106**, 18249–18254.
67. Reynolds, K.A., McLaughlin, R.N., and Ranganathan, R. (2011). Hot spots for allosteric regulation on protein surfaces. *Cell* **147**, 1564–1575.
68. Gunasekaran, K., Ma, B., and Nussinov, R. (2004). Is allostery an intrinsic property of all dynamic proteins? *Proteins* **57**, 433–443.

Current Biology, Volume 24

Supplemental Information

**A Comprehensive Biophysical
Description of Pairwise Epistasis
throughout an Entire Protein Domain**

C. Anders Olson, Nicholas C. Wu, and Ren Sun

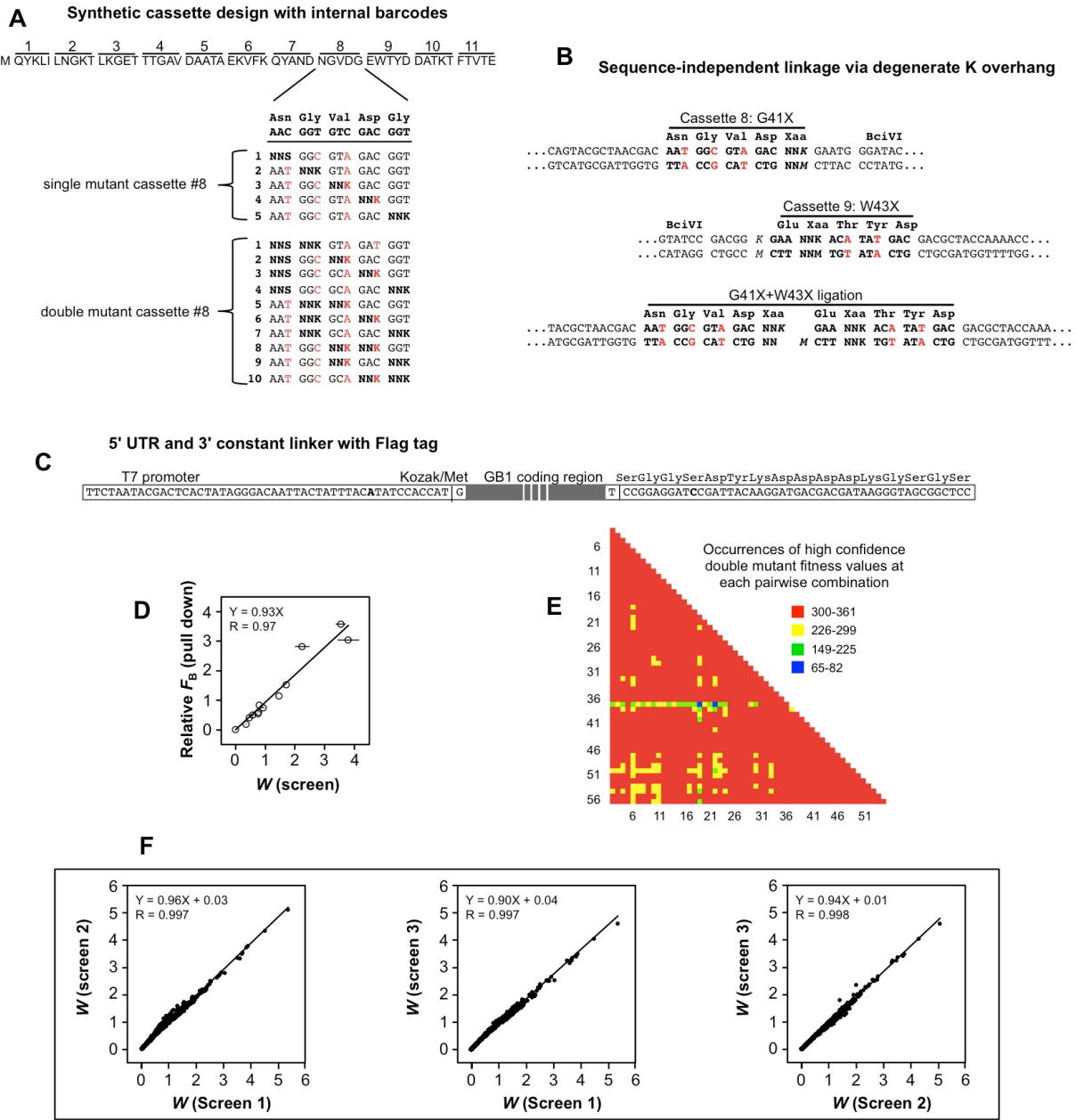
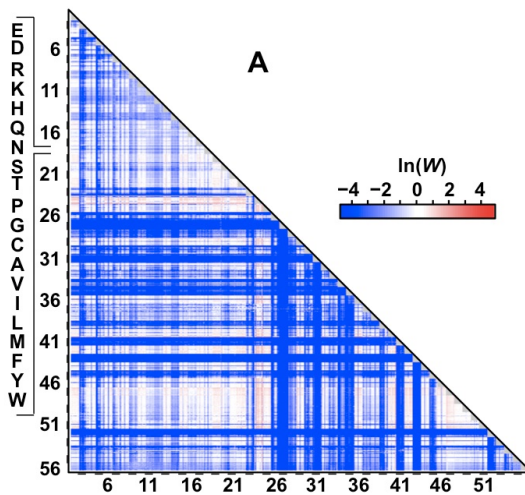


Figure S1. Library design and affinity based fitness. Related to Figure 1 and Table S1. (A) Cassette design. The 55-residue random region was split into 11 cassettes. Oligonucleotides were designed to randomize each codon singly or each codon pair within each cassette. (See Table S1 for all oligonucleotide sequences). We needed to devise an error correction method because the paired end reads (100 bases from each end) were not entirely overlapping (however the entire amplicon was fully sequenced by pairing reads, thus enabling identification of distant mutations). Therefore we made changes in sequence (red) compared to the template at the third base of codons in order to create an

internal barcode that enabled distinguishing randomized positions from sequencing errors (cassette 8 shown for example). (B) Sequence-independent cassette ligation. A type II^s restriction enzyme (BciVI) was utilized to leave a single base overhang after digestion that enabled joining randomized or wild type cassettes. G or T (K) was used at the third base position to cover all possible amino acids when the final residue of the cassette was randomized while also enabling specific ligation between adjacent cassettes. The 3' fragment, whether random or constant, contained a complementary degenerate base “M” (A or C) as the overhang. The library sequence was designed to eliminate any possible occurrences of BciVI within coding regions. (C) Library 5' and 3' design. The 5' UTR and 3' constant linkers contains a “hidden” BciVI site. After selection, primers change the base in bold to match the BciVI recognition sequence. This enabled ligation with custom Illumina adapters that contained a complementary overhang and eliminated the need to sequence non-random termini, except for the single overhang base used for ligation (boxed). (D) Fitness validation. Binding fitness was validated by a ³⁵S-Methionine-labeled pull-down assay. Thirteen variants were reconstructed (see Table S1) and expressed *in vitro* for validation of binding fitness. The variant binding efficiencies were measured by scintillation counting of input and washed beads after binding. The fraction bound normalized to wild type fraction bound ($F_{B,mut}/F_{B,wt}$) was compared to W from the screen. The average value of W from the triplicated screen is shown with error bars representing the standard deviation. A single, representative pull-down value is shown. Triplicated pull-down experiments required conversion to $\Delta \ln(K_A)$ as experimental variability in target concentration created variability in $F_{B,mut}/F_{B,wt}$ which was resolved by accounting for the curvature of binding isotherms (see the Experimental Procedures). (E) High confidence coverage throughout GB1. 99.97% of all possible double mutants (535,917 of 536,085) were observed in the input pool and 95.1% of all double mutants were observed with high confidence as determined by a Poisson-based 90% confidence interval by accepting $W_{high} - W_{low} \leq 0.1$ or $\ln(W_{high}) - \ln(W_{low}) \leq 0.5$ (see below and the Experimental Procedures). There are $19 \times 19 = 361$ possible double mutants for each pairwise position combination (1485). Examples of high confidence double mutant fitness values are distributed throughout all 1485 possible position combinations enabling determination of epistasis throughout the domain. (F) Reproducibility of fitness calculation. The correlations between single mutants fitness values from each of the three separate binding screens are displayed. All variants were highly correlated in screens 2 and 3. Eight variants at the first random position (Q2) in screen #1 displayed artificially low counts compared to screens 2 and 3. Because the sequencing counts in screens 2 and 3 were sufficient this artifact did not affect the calculation of fitness for these 8 variants.



B Streptococcal protein G homologs

	6	11	16	21	26	31	36	41	46	51	56
GB1 (GC1, G β 1)	TYKLILNGKTLKG	TTEAVDAA	TAEKVFKQY	ANDNGV	DGEWTY	DDATKTF	TVTE				
GC2	VI.....
GB2 (GC3)	VI.....
Mag, MIG D5	VI.....
ZAG D2	R.VIK.V.FS...A.K.QT.R.IT.A.T.
ZAG D1	S.VIK.A.FS...A.K.QT.RD..K.V.A.A.
MIG D4	V.K.N.FS...K.E.A.E.Y.S.
MIG D1	VVK.N.FS...K.I.T.E.TA.N.S.

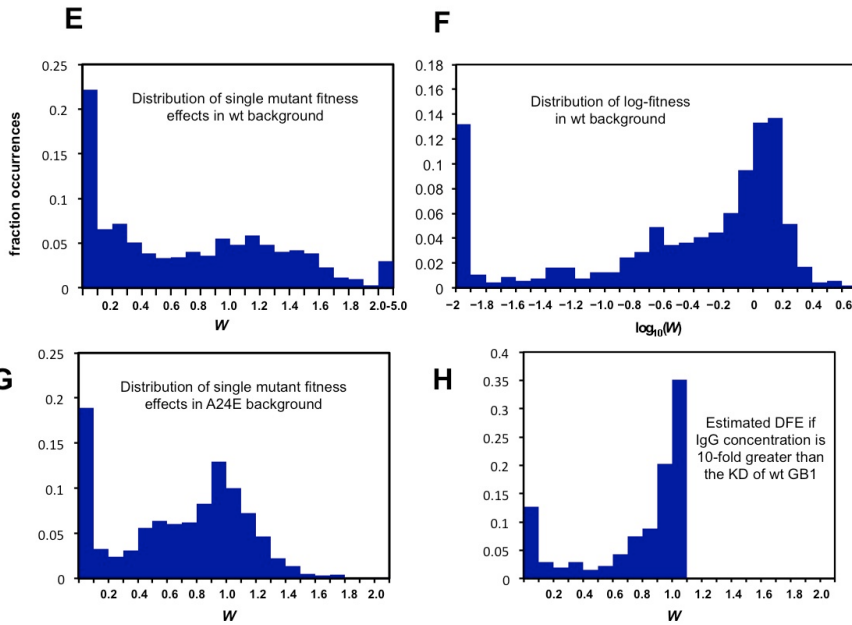
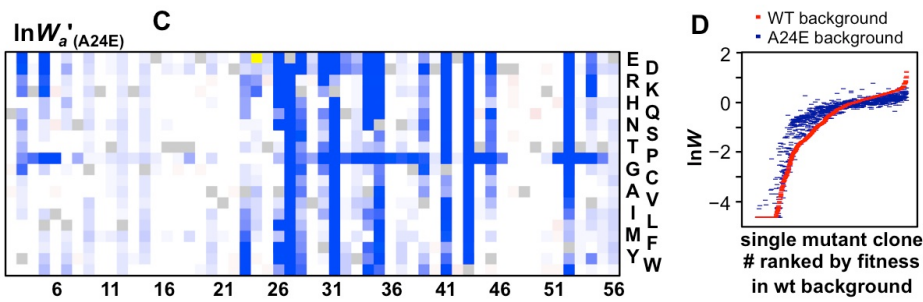


Figure S2. Fitness maps and distribution of fitness effects. Related to Figure 2. (A) Fitness map of double mutants by position. The amino acid order within each pair is listed to the left of the figure panel (the wt amino acid is excluded). Up to $19 \times 19 = 361$ amino acids are displayed per each of the 1485 pairs depending on the confidence (see Figure S1E). (B) GB1 compared to Streptococcal IgG-binding domains from proteins: MIG [S1], MAG [S2], and ZAG [S3]. Protein G is composed of tandem repeats of either 2 (GB1 and GB2) [S4] or 3 (GC1, GC2, and GC3) [S5] IgG binding domains. GB1 is identical to the C1 domain and GB2 is identical to the C3 domain. GB1 is also referred to as G β 1 [S6]. As can be seen in Figures 1B and 2A, there are numerous positions where wt is not optimal (35% of single mutants display $W > 1$). One reason for this lack of optimization is likely a result of the propensity for GB domains to repeat in tandem [S7] and therefore protein G likely achieves sufficient affinity through avidity effects. The protein G homolog MAG contains only one GB domain however which might create a demand for increased affinity. The 7 amino acid differences between MAG and GB1 are all adaptive in our screen, and it includes A24E, which is the most beneficial mutation that can be achieved by one DNA base change. Furthermore MIG domain 4 contains A24E in addition to the most improved single base substitution outside of position 24 (D40Y). (C) The fitness of all mutations in the A24E background. While the number of beneficial mutations is nearly the same, magnitude of beneficial effects is noticeable smaller. (D) The fitness as in panel C compared to the wild type fitness profile. The profile flattens slightly because the parental (A24E) K_D is closer to the IgG concentration. Beneficial mutations produce diminishing fitness effects in this background and deleterious mutations demonstrate a smaller effect due to decreased stringency. We did not directly determine the concentration of IgG-FC in the experiment, but we can extrapolate from binding data to predict $[IgG] \sim 0.14$ -fold the wt GB1 K_D . We estimate A24E has a 5.5-fold better affinity than wt GB1 (see the Experimental Procedures). (E) The distribution of fitness effects (DFE) is broad and relatively flat in this stringent functional test, unlike the typical distribution *in vivo* [S8, S9]. (F) The DFE is sometimes created by binning $\log(W)$, and doing this produces a similar shape in our DFE as those shown by Firnberg *et al.* [S10] and McLaughlin *et al.* [S11]. (G) The DFE in the background of A24E. The flatter profile observed in panel D produces a more noticeable peak around neutral fitness. (H) We can predict how affinity produced fitness in less stringent environments by using the relationship between K_D and fraction bound at different target concentrations. Thus we estimated the fitness of each single mutant if the concentration of IgG were 10-fold higher than the K_D of wt GB1. This produces a more typical DFE [S8, S9] as the beneficial mutations are essentially neutral (maximum $W = 1.09$) and the functional test is less stringent for lower affinity variants.

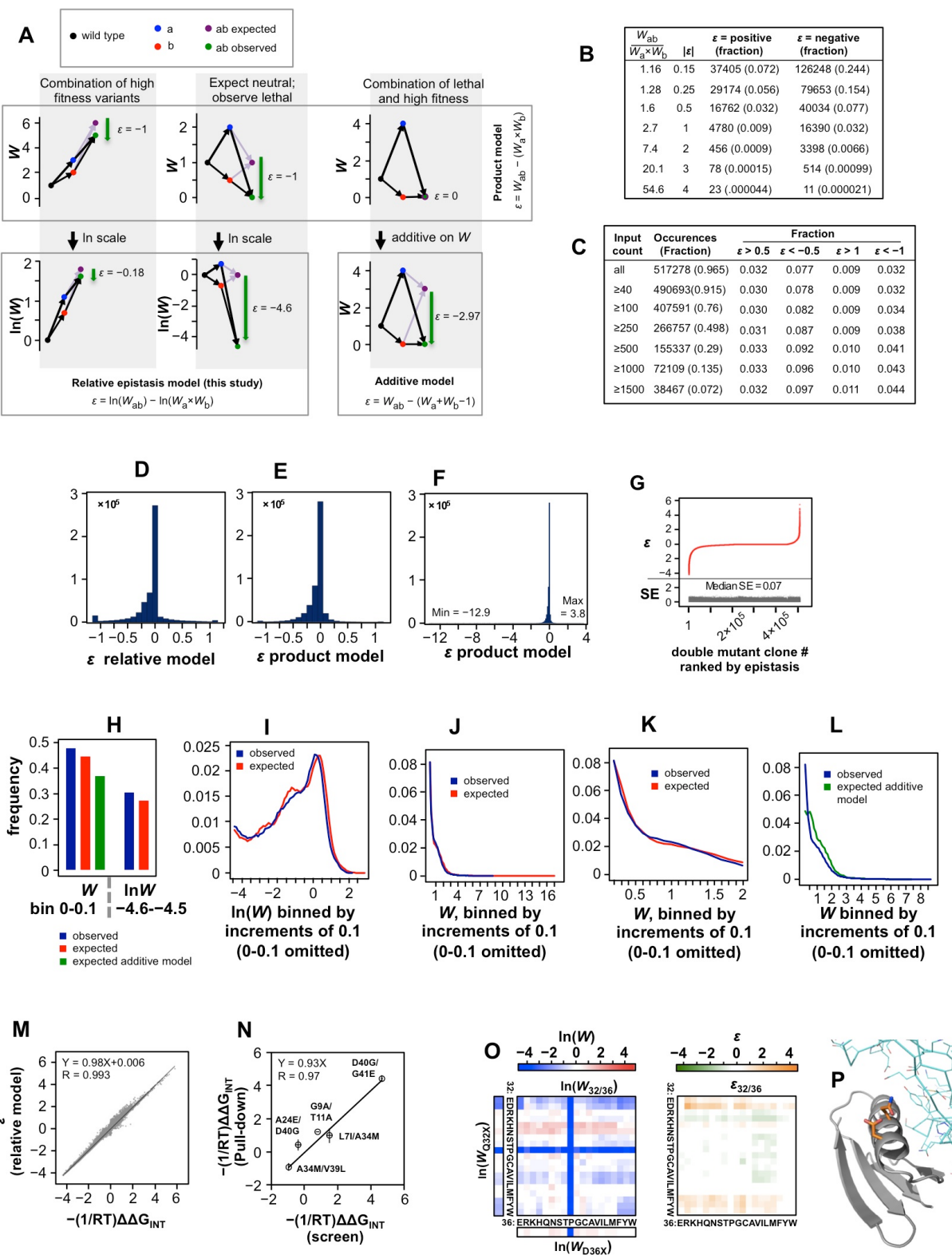


Figure S3. Models of epistasis. Related to Figure 3. (A) We show a few hypothetical examples of fitness pathways that demonstrate how different models of epistasis produce different values of epistasis. Both the product model and a relative model of epistasis predict that double mutant fitness will be the product of the individual constituent mutations [S12-14]. The product model determines the absolute difference between observed and expected. In our adaptation experiment, we observe double mutants that are significantly more fit than wt GB1. Therefore a very beneficial double mutant can display the same value of negative epistasis as a lethal double mutant even if the lethal mutant is expected to be as fit as wild type. In terms of absolute numbers of “progeny” the difference in observed and expected is the same in the two examples. However, we are interested in how significantly the fitness of mutants change in alternative backgrounds such as is shown in Figure 2C,D, thus we use a relative model of epistasis which is the ratio of expected to observed and is therefore additive on log scale. Another model of epistasis is the additive model which expects double mutant fitness to be the sum of the individual fitness effects scaled by -1 [S13, S14] (or it can be considered to be a sum of the constituent selection coefficients (s) and plus 1 to convert back to W). This model will reduce the magnitude of diminishing returns epistasis, but will create large negative epistasis values for all combinations of lethal mutants and beneficial mutants (see also panel L below). This model will also not show positive epistasis when a lethal and a beneficial combine to produce a beneficial mutant. (B) The fraction of negative and positive epistasis exceeding different magnitudes. To help visualize the significance of epistasis values we provide the relative change in fitness [$\text{expected}/\text{observed}$ or $W_{ab} \div (W_a \times W_b)$] for each category. Theoretically, relative epistasis can range from $\pm\infty$ depending on the sensitivity of the binding assay and the sensitivity of the detection method. The largest fold decrease observed in our screen is 67-fold and the largest increase is 230-fold. Note that $W_{ab} \div (W_a \times W_b)$ is approximately equal to $\varepsilon+1$ for $|\varepsilon|<0.5$ because in this range $e^x \approx x+1$. Therefore values of $|\varepsilon|<0.5$ represent the approximate fraction increase or decrease from the expected fitness. While these are small in magnitude relative to the largest examples of epistasis, fractional changes are also significant in evolutionary pathways (see Figure 7). (C) The effect of increasing sampling on negative and positive epistasis. As input variant frequencies increase, the fraction displaying epistasis does not change significantly showing that our confidence interval is effective. (D) A histogram showing the distribution of epistatic effects (see Figure 3C) with a limit combining $|\varepsilon|>1.05$ to highlight the distribution of smaller effects. (E) The distribution of epistatic effects using the product model with a limit $|\varepsilon|>1.05$. Large epistatic effects are also rare in this model; however, the significance of different values is obscure relative to the fitness of the double mutants as described in panel A. (F) The full distribution of epistatic effects from the product model showing substantial diminishing returns epistasis from the product of highly beneficial mutations which would predict binding function that is impossible. In a well adapted landscape such as what is predicted if the [IgG] concentration was higher (see Figure

S2H) or affinity of the parent was higher, this model would not produce such unrealistic expectations. (G) The profile of high confidence double mutant epistasis compared to the standard error of double mutant $\ln(W)$ from the triplicated screen. The median value of standard errors is 0.07. (H-K) The expected double mutant DFE close matches the observed. (H) We separated the lowest bin from the distributions as this is by far the most common category. The product and log-scale distributions predict slightly less lethals which fits with observations about the nature of negative epistasis (see below). The additive expectation predicts even less lethals than is observed as is shown in panel A. (I) The DFE is binned by $\ln(W)$ and thus there is a peak of distribution around neutral fitness as in Figure S2F. (J) The expected distribution includes very small fractions of unrealistic high fitness mutants. This tail is compressed by the log-scale fitness distribution in panel H. (K) The DFE of expanded between 0.1 and 2 to show the expected DFE is very similar to the observed. (L) The DFE predicted by the additive model expects significantly less lethals and significantly more beneficial double mutants. (M) Under the conditions of this screen where $[IgG]$ is less than the K_D , non-additivity in fitness effects resulting from additive energetic effects is predicted to be small compared to significant examples of epistasis. (N) The 13 variants constructed and tested for binding fitness validation (Figure 2A) include 5 double mutants and 8 constituent single mutants. $\Delta\Delta G_{INT}$ derived from the pull-down assay was calculated for these 5 double mutants and compared to the screen values. The error was calculated as the root sum of squared standard deviations of both single mutant fitness and the double mutant fitness values from either the triplicated screen or triplicated pull-down experiment. (O) Enlarged $\ln(W)$ and ε map for interactions between α -helix residues 32 and 36 displaying both positive and negative epistasis. Both are on the surface of the α -helix in position to interact ($i, i+4$) and are adjacent to the binding surface (Figure 3G). Dramatic positive epistasis occurs between Q32D/E and substitutions for Asp36, demonstrating rescue of very low fitness acidic substitutions at position 32 by removal of an unfavorable electrostatic interaction with Asp36. Interestingly, an example of such a permissive mutation (32D/36K) is observed in ZAG, a homolog of GB1 (Figure S2B). (P) Structure of GB1 bound to IgG-FC highlighting wt residues Q32 and D36 (PDB 1FCC) [S15].

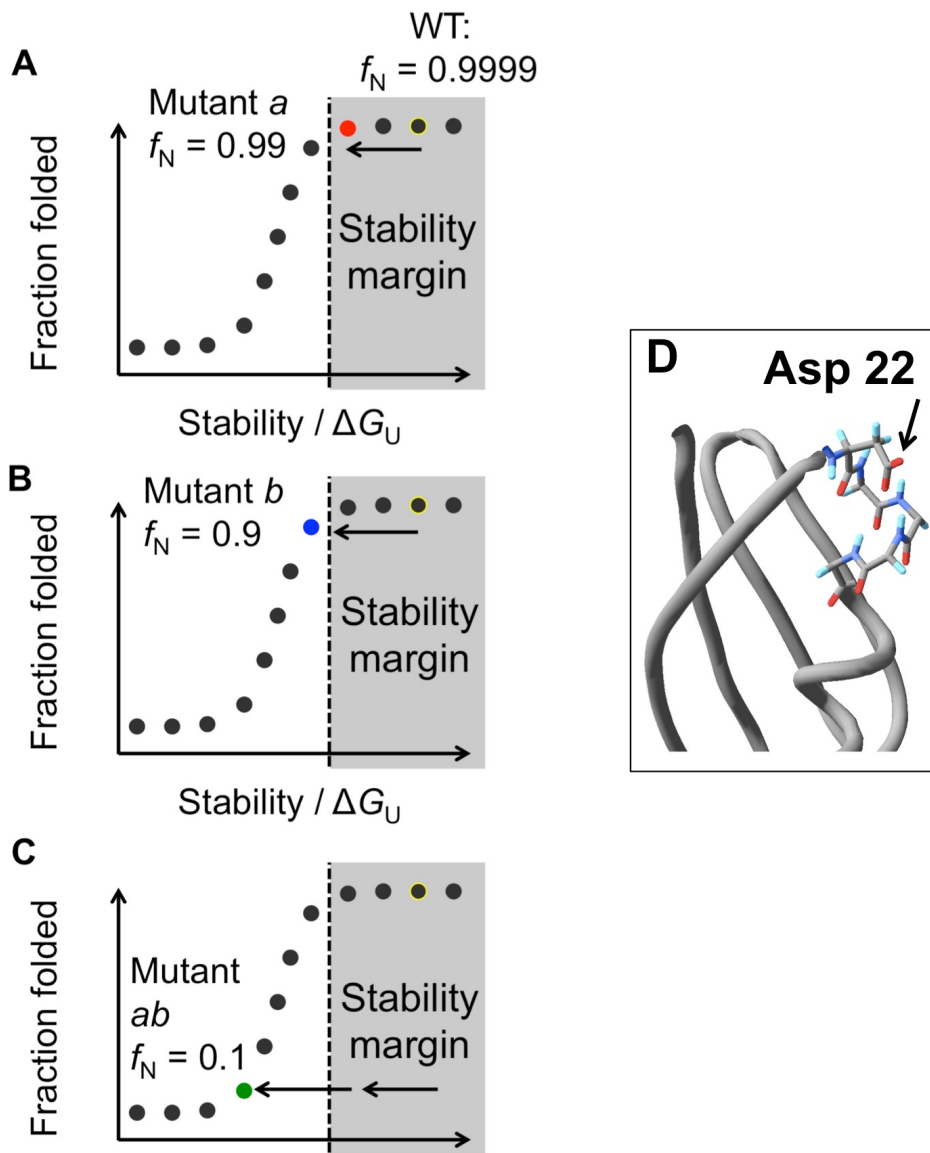
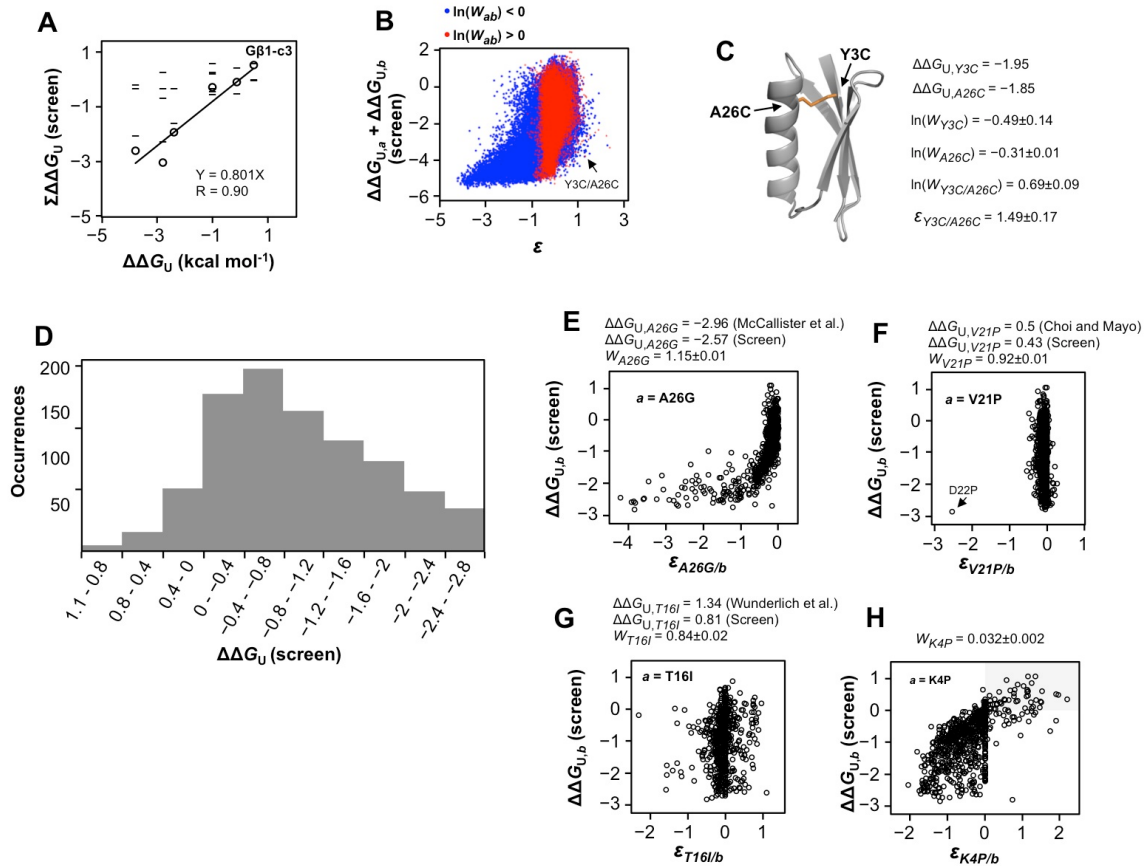


Figure S4. Theoretical mutations that display the threshold robustness effect. Related to Figure 4.

(A) Wild type here is depicted to be 99.99% folded while one mutation (*a*) is significantly destabilized yet falls within the stability margin and is thus nearly as folded as wt (99%). In this scenario, the magnitude of destabilization is approximately half of the difference in energy between the folded and unfolded state and yet the decrease in native protein is negligible. Note that most mutations will fall within the stability margin [S16] and thus stability and fitness will not be correlated (see below, Figure 5A). (B) Another theoretical mutation (*b*) is slightly more destabilizing than mutation *a* and having slightly surpassed the stability threshold is 90% folded. (C) The two mutations that each largely exhaust

the stability margin together significantly unfold the protein. The additive stability effects produce a strong functional epistatic effect due to the cooperative nature of protein folding as the double mutant is only 10% native and 90% non-functional. (D) The interaction between the helix N-cap residue Asp22 side chain and the helix N-terminus is highlighted. Asp22 H-bonds with the Thr25 NH and may further stabilize the helix through interaction with the helix macrodipole. Note that substitutions for Asp22 with Asn, Thr, and Ser display lower magnitudes of epistasis in combination with polar substitutions at position 5 (Figure 4C) as expected if these neutral side-chains preserve the main-chain H-bond but do not stabilize the helix macrodipole. Substitutions with Cys also display lower negative epistasis even though Cys is not typically seen in capping motifs [S17]. However, N-capping through a Cys thiolate has been shown to stabilize model helices and is likely rare at such positions in nature due to thiolate reactivity [S18, S19]. Thus, the range in functional epistasis observed between substitutions at positions 5 and 22 is consistent with anticipated stability effects.



$\ln(W_{K4P}) = -3.43 \pm 0.05$							
Stabilizing mutation (<i>b</i>)	$\Delta\Delta G_{U\text{-screen}}$	$\Delta\Delta G_{U\text{-literature}}$	$\ln(W_b)$	$\ln(W_{K4P/b})$	$\epsilon_{K4P/b}$	90% CI min	
T16W	1.06		-1.19 ± 0.03	-3.21 ± 0.13	1.41 ± 0.15	1.33	
D40Y	0.86		1.21 ± 0.07	-0.91 ± 0.02	1.30 ± 0.08	1.24	
I	T16I	0.81	1.34	-0.18 ± 0.03	-2.74 ± 0.13	0.87 ± 0.58	0.86
N37L	0.64	1.43	-1.18 ± 0.08	-3.70 ± 0.21	0.91 ± 0.23	0.79	
V29Y	0.64		0.06 ± 0.02	-2.15 ± 0.25	1.23 ± 0.26	1.12	
L12F	0.63		-0.98 ± 0.05	-3.55 ± 0.18	0.86 ± 0.19	0.67	
E19F	0.59		0.45 ± 0.04	-1.39 ± 0.24	1.59 ± 0.24	1.51	
L7I	0.58		0.53 ± 0.001	-1.71 ± 0.09	1.18 ± 0.10	1.12	
T16L	0.58	1.08	-0.27 ± 0.01	-3.28 ± 0.10	0.42 ± 0.11	0.37	
.....							
J	T25E	-0.04	0.48	-1.04 ± 0.03	-4.23 ± 0.37	0.24 ± 0.37	0.12
T18L	-0.09	0.33	-0.53 ± 0.02	-4.29 ± 0.31	-0.33 ± 0.31	-0.17	
T53Y	-0.36	0.06	-0.53 ± 0.04	-4.37 ± 0.26	-0.41 ± 0.27	-0.17	

Figure S5. Additive and non-additive stability effects and epistasis. Related to Figure 5, Table S4 and Table S5. (A) $\Delta\Delta G_U$ for multiple mutants published in the literature was predicted by summing $\Delta\Delta G_U$ from the screen (see Table S5). Multiple mutant values are identified by open circles while the $\Delta\Delta G_U$ values for constituent single mutations are shown as dashes. Our $\Delta\Delta G_U$ values predict the

enhanced stability of the engineered triple mutant G β 1-c3 [S20]. We cannot however predict stability of the hyperstabilized seven-fold variant G β 1-c3b4 [S20], or the four-fold hyperstabilized variant G β 1-M2 [S21] (see Table S5). Also, non-additive effects are not predictable such as those described previously [S22-24]. (B) Comparison of $\Delta\Delta G_{U,a} + \Delta\Delta G_{U,b}$ to epistasis. Most variants displaying severe negative epistasis are severely destabilized relative to wild type. However, many variants predicted to be unstable display minimal epistasis, showing non-additivity in stability effects or overestimation of deleterious stability effects. For example, Y3C/A26C is a beneficial double mutant predicted to be very unstable as two buried core residues are mutated. (C) A model of the Y3C/A26C variant that might form a disulfide bond, thus explaining non-additivity in stability effects. This double mutant illustrates how cooperativity in thermodynamic stability might produce positive epistasis in binding fitness as both single mutants are deleterious alone. (D) Histogram displaying occurrences of predicted stability effects (average values from the five reference backgrounds). Most mutations are slightly destabilizing as expected [S16]. Only a few mutations are moderately stabilizing while numerous mutations are severely destabilizing, explaining the abundance of negative epistasis relative to positive epistasis (Figure S3B). The ability to predict stability effects becomes more difficult as fitness decreases and thus this analysis is limited to the 709 of 1045 mutations that display $W > 0.24$. (E) The relationship between epistasis and stability of mutations in combination with A26G. This mutation was chosen to highlight the impact of the threshold robustness effect as it is a neutral mutation predicted to be unstable from the screen data and also shown to be destabilizing in the literature [S25]. The relationship matches the conclusion shown in Figure 5C. There is notably no positive epistasis with the destabilizing residue considering it is predicted to be folded at the screen temperature. (F) Epistasis versus stability of residues combined with V21P which is predicted to be moderately stabilizing by the screen and confirmed to be stabilizing in the literature [S26]. Significant epistasis is not observed with these pairs because the destabilizing mutations are predicted to be folded at the screen temperature. Even for partially folded mutants the effect is small: the epistasis observed between V21P and the background mutants are 0.24 (Y3A), 0.42 (Y3C), 0.19 (L5N), 0.09 (L5S), and 0.2 (F30N) (values are raw epistasis values, not minimized by the confidence interval). (G) GB1 has served as a model protein for protein folding and stability with multiple studies on design or selection of stabilizing mutations [S20, S21, S27]. One of the most stabilizing residues identified in the literature and in the screen data is T16I. This residue displays numerous epistatic interactions but this is not correlated with stability of the partners. Furthermore, many other substitutions for T16 are also stabilizing but the amount of epistasis between these and destabilized core substitutions is very small (compare epistasis within 3, 5, 22, 26, 30, 46, and 51 and those between 16 in Figure 3A,B). The epistasis values observed between T16I and the background mutants used to calculate thermodynamic stability are 0.37 (Y3A), 0.36 (Y3C), 1.17 (L5N), 0.55 (L5S), and 0.93 (F30N) (values are raw epistasis values, not minimized by

the confidence interval). We note that despite different epistasis values the backgrounds produce very similar stability values (except for T16I/L5N which cannot be used to calculate $\Delta\Delta G_{U,T16I}$): $\Delta\Delta G_U = 0.77$ (Y3A), 0.93 (Y3C), 0.80 (L5S), and 0.73 (F30N). T16I/L5N does not satisfy the condition of non-additivity as $W_{T16I/L5N}/W_{T16I} > 1$ and our method cannot be used when $W_{ab} > W_b$. This is rare and this occurrence is the only example of $W_{L5N/b} > W_b$ among the 82 variants in the literature in the L5N background. (H) Stabilizing mutations should display the largest epistasis with substantially destabilized variants that are largely unfolded. To illustrate this we show how mutations produce epistasis in combination with K4P in relation to stability. Lysine 4 is a solvent exposed residue in the middle of β -strand 1 far from the FC binding site. The proline substitution abolishes a main-chain H-bond with the adjacent parallel strand 3 thereby disrupting the β -sheet and thus is predicted to be substantially unfolded, but not completely as W is measurable. (In contrast no mutations are stabilizing enough to rescue T53P which has been demonstrated to be unfolded [S6, S28] and displays $W_a < 0.01$ as the maximum double mutant fitness is <0.04). Significant epistasis is observed between K4P and stabilizing mutations, as well as additional neighboring substitutions that may display non-additive stability effects. (I) The epistasis values between the most stabilizing mutations predicted by the screen and K4P are listed. All stabilizing mutations display positive epistasis with K4P as expected if they act similarly to increase the fraction of protein that is folded in the K4P background. The highest fitness double mutant including K4P is in combination with the stabilizing and beneficial mutation D40Y which increases the observed fitness ($W_{ab} = 0.40$) approximately 4-fold compared to the expected fitness ($W_a \times W_b = 0.11$). (J) We also show additional variants reported to be stabilizing in the literature that do not match our prediction. These mutations also do not stabilize the K4P background as do the substitutions predicted to be stabilizing by the screen. Thus experimental variability [S29] or differences in background mutations [S6, S28] could explain the substitutions that do not agree.

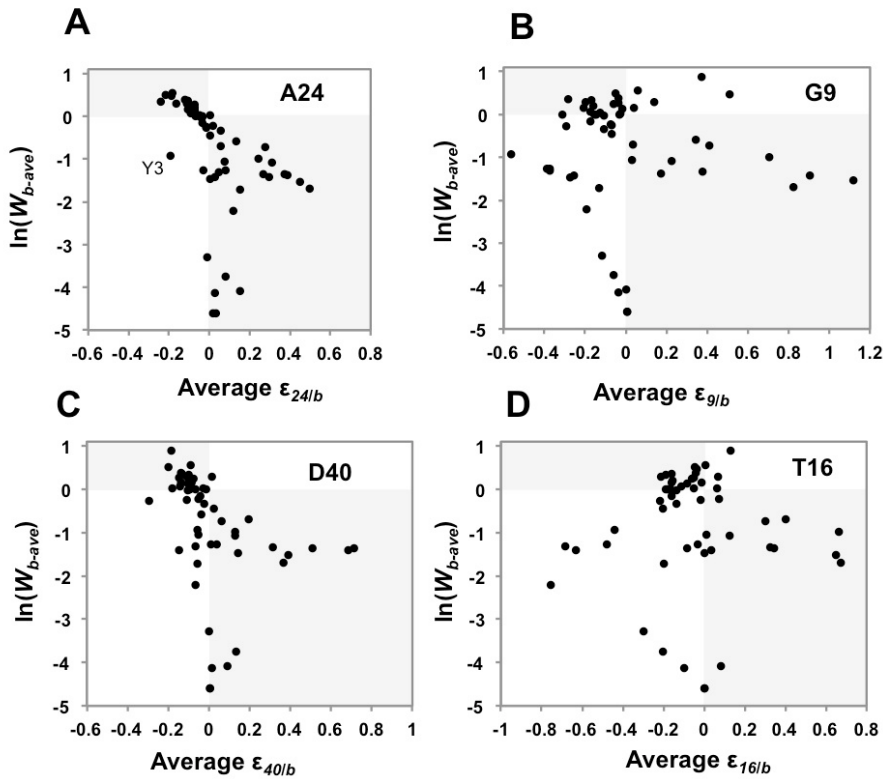


Figure S6. Positions that display positive epistasis in general and highly diverged protein G-like domains are found in other species. Related to Figure 6. (A) The numerous highly beneficial substitutions at position 24 display positive epistasis with positions that are deleterious on average and negative epistasis with positions that are beneficial on average (see Figure S2C-D). (B-D) Other positions that display positive epistasis in general within a conformationally dynamic network of residues do not show this trend. G9 is very sensitive to substitution on average while substitutions at D40 are highly beneficial. T16 is moderately sensitive to substitution on average and many substitutions are highly stabilizing. (E) Representative domains are shown from *Lactobacillus iners* (GenBank: EFU78259.1), *Alloioococcus otitis* (GenBank: EKU92966.1), and *Eremococcus coleoccola* (GenBank: EFR31353.1). In addition to containing tandem repeats of GB-like domains, these proteins contain domains homologous to

albumin-binding “GA” modules also found in streptococcal protein G (not shown). Numbering corresponds to the GB1 sequence. Highly conserved positions are highlighted in dark grey and similar residues are highlighted in light grey. These coincide with structurally important core residues and residues in the two stable loops (β 2- α and β 3- β 4). Insertions are found in most domains at one or both of the flexible loops. One domain from *L. iners* however contains an identical number of residues as GB1. The most extreme example of positive epistasis in our screen is produced by the combination of G41L and V54G, which coincides with the identity of this *L. iners* domain (bold).

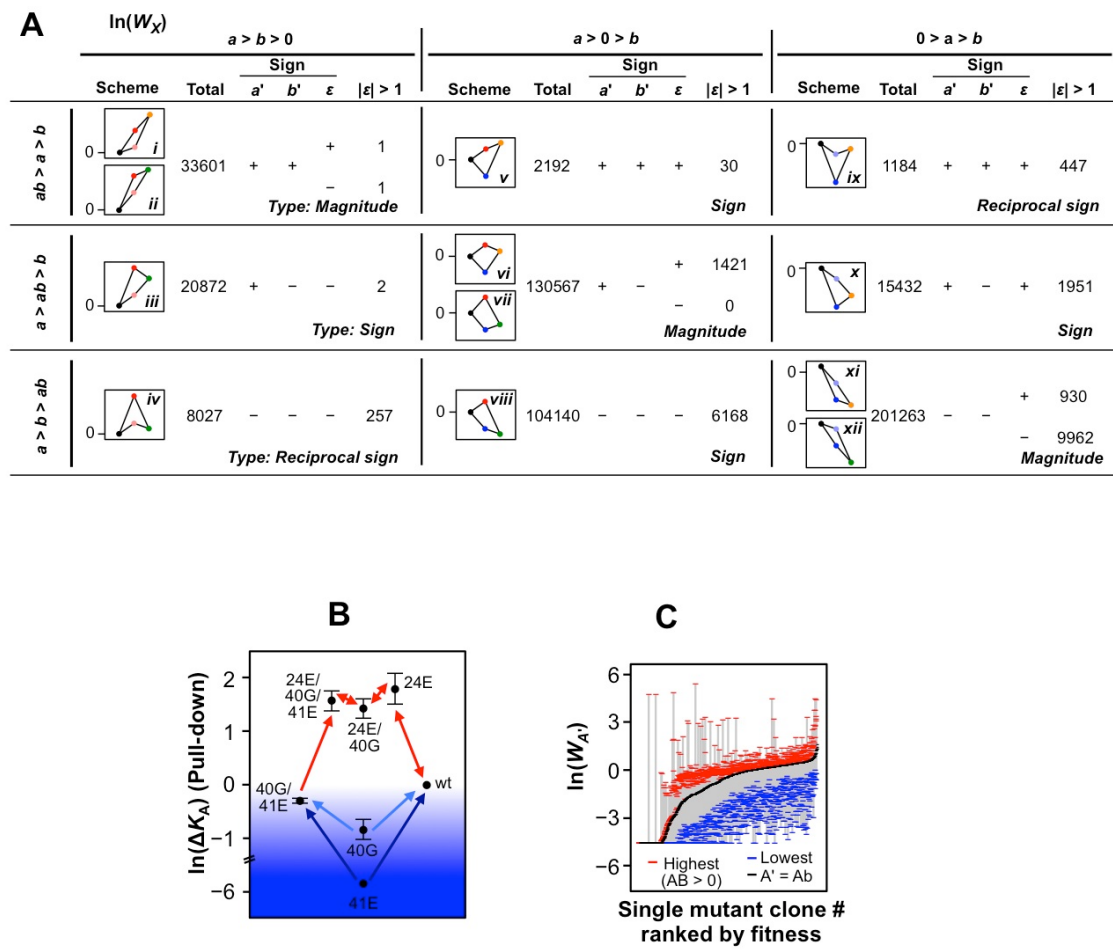


Figure S7. Impact of epistasis on the GB1 double mutant fitness pathways. Related to Figure 7. (A) Schemes *i-xii* show how deleterious or beneficial mutations combine to produce lower, intermediate, or higher fitness than the constituent mutations and count the number in each category that demonstrate $|\varepsilon| > 1$. The color scheme matches that of the heat maps for fitness (a or b) or epistasis (ab). “Sign

epistasis” occurs if the sign of $\ln(W)$ changes for one mutation while “reciprocal sign epistasis” refers to a change in sign for both mutations. Magnitude epistasis can exacerbate deleterious mutations, enhance beneficial mutations or minimize the effects of either. Negative epistasis is most common when two deleterious mutations produce magnitude epistasis (scheme *xii*) and when one deleterious and one beneficial mutation produce sign epistasis (scheme *viii*), which is expected considering the stability effects described above (Figure 5C). A large fraction of positive epistasis occurs when the combination of two deleterious mutations results in a reversal in fitness for one variant although these produce a double mutant less fit than wild type (scheme *x*). A significant fraction of positive epistasis occurs when one variant is partially compensated by a beneficial mutation (scheme *vi*) and when two deleterious mutations partially reduce the deleterious effect of each (scheme *xi*) which is characteristic of many mutations within the dynamic network (Figure 6B). Reciprocal sign epistasis is an extreme case of either negative epistasis (scheme *iv*) or positive epistasis (scheme *ix*) that can result in isolated local fitness optima. Negative reciprocal sign epistasis represents a potential for fixation of suboptimal fitness in adaptation (scheme *iv*). Reciprocal sign epistasis between two deleterious mutations could represent a local optimum avoided in an adaptive path to the current genotype or a potentially inaccessible path to greater fitness (scheme *ix*). Nonetheless, considering the multidimensionality of protein sequence space, it may be possible to circumvent a valley through a high fitness ridge (B). The variants listed were reconstructed and expressed *in vitro* with a 35S-Methionine label to determine binding efficiency as in the validation experiment. Error bars indicate the standard deviation of the triplicated pull-down experiment. The permissive background, A24E, is found naturally in the higher fitness B2 domain. (C) The fitness values of many mutations change dramatically depending on the background in which they appear. The range is bound by a blue dash for the lowest fitness in any of the 1026 possible alternate backgrounds, and by a red dash for the highest fitness only for double mutants with $\ln(W)>0$. Thus, only beneficial double mutants are shown for each maximum $\ln(W_a')$ value.

SUPPLEMENTAL TABLES

Table S1: Oligonucleotide sequences. Related to Figure 1 and Figure S1.

Template construction primers

```

GT1FOR GGACAATTACTATTCACATCCACCATGCACTAACGGTATCTGAACCGTAGCAG
GT2FOR GCTGATTCTGAAACGGTAAAGCGCTAAAGGGTGAGACGCCAACGGCTGAAGCTGAGAC
GT3FOR CACCGAAGCTGTAGACGCTGCTACTGCAGAGAAGGTGTTCAAGCAGTACGCCAACGAC

```

```

GT4REV  AGCGCTCTGGTAGGTCATTACCGTCGACAGCGTTCGGTAGGCTGACTCTGGAACAC
GT5REV  TCGGATCTCCGGATTCTGGAACTGGTAAAGGTTGGTAGCGTCGTCTGAAGGTCATTC
GT6REV  GGAGCCGCCTACCCCTATCGTCGTACCTTGTAAATCGGATCCTCCGGATTCCG

```

Mutagenic primers

G11R24FOR	GACGACGTATCCAAAACCTTTNNKGTAACGGAGGATCCGA	G11R35FOR	GACGACGTATCCAAAACCTTTACCNKACCNKTCGGAGGATCCGATTAC
G11R25FOR	GACGACGTATCCAAAACCTTTNNKGTAACCGAGGATCCGATTAC	G11R45FOR	GACGACGTATCCAAAACCTTTACCNKNNKGTAATCGGAGGATCCGA
Constant primers			
G1CREV	AGCGTGTATCCTTCAGAATCAGTTGACTGCATGG	G2CFOR	ATGCAGGTATCCCTGATKCTGAACGGTAAGACGCTGA
G2CREV	GTCGTGTATCCTTCAGCTCTTACCGTTCA	G3CFOR	ATTCCTGTTATCCAAGACKTGAAGGTGAGACGACCAC
G3CREV	TCTACAGTATCCCGTGTCTCACCTTCAG	G4CFOR	ACGCTGGTATCCGAGACKACCCGAAGCTGTAGACG
G4CREV	TCTCGAGTATCCCGTCAACAGCTCGGTGGT	G5CFOR	ACGACCGTATCCGCTGTGACGCTGCTACTGCAGAG
G5CREV	TGCTTGTTATCCCTCTCAGCAGTCAGCGTC	G6CFOR	GTAGACGTATCCACTGCKGAGAAAGGTGTCAGCAGTAC
G6CREV	CCGTTGTTATCCCTACTGCTTGAACACCTTC	G7CFOR	GCAGAGGTATCTTCAAKCAGTACGGTAACGACAACCG
G7CREV	GGTCATTACCGGTATCCCCTTATCGTTAGCGTACTG	G8CFOR	AACGAGGTATCCAACGAKAACCGTGTGAAATG
G8CREV	TCTCGGTATCCCATTCACCGTCACCGTT	G9CFOR	GACAAAGGTATCCGAGCTGKAATGGACCTACGACGACG
G9CREV	AAAGTTGTTATCCGCTCATCGTAGGTCATT	G10CFOR	GGTGAAGTATCTACAGKAGACGCTACAAAACCTTCAC
G10CREV	GATTCCGGTATCCGTGAAAGTTTGTAGCGTC	G11CFOR	GACGAGGTATCCAAAACCTTACCGTTACCGAATCC
Cassette fill-in primers			
GF1REV	GGAGCGTCGTATCCCTCAG	GF2FOR	CCATGCAGGTATCCCTGAT
GF2REV	GGTGTGCGTATCCCTCAG	GF3FOR	CCATTCTGTTATCCAAGAC
GF3REV	GGCTCACAGTATCCGTTGGT	GF4FOR	CACGGTGTATCCGAGAC
GF4REV	TCTGCAGTATCCCGCTC	GF5FOR	ACGACCGTATCCGCTGT
GF5REV	CCCTGCTGTTATCCCTC	GF6FOR	CGTAGACGTATCCACTG
GF6REV	CCCTGTCGGTATCCCTACTG	GF7FOR	CCCGAGAGGTATCCCTCAA
GF7REV	CCATTACCGGTATCCCCGT	GF8FOR	GCAAGCAGGTATCCAACGGA
GF8REV	CCCTGTCGGTATCCCATTC	GF9FOR	CGAACACGTATCCGACGT
GF9REV	CCAAGTTGTTATCCGCTC	GF10FOR	CCGGTGAAGTATCTACAG
GF10REV	GGGATTCCGGTATCCGTGA	GF11FOR	CCGACGACCTATCCAAAAC
Selection primers/oligos			
T7BCIVI-	TCTTAATACGACTCACTATAGGGACAATTACTATTATCCACCATG	SPLINT	TTTTTTTTTTGGAGCCGCTACC
T7BCIVI+	TCTTAATACGACTCACTATAGGGACAATTACTATTACGTATCCACCATG	LINKER	5' phospho-d(A)21-(9)3-ACC-Puromycin
LIBREV	GGAGCCGCTACCCCTATCGTCG		
5' BCIVIREV	CCTTATCGTCGTATCCTGTAAATCGTATCCCTCCGGA		
Validation primers			
7IFOR	CCATGCAGTACAAGCTGATTATCACCGTAAAGACG	39LFOR	CGACAAACGGTCTCGACGGTGA
9AFOR	CCATGCAGTACAAGCTGATTCTGAACGCTAAAGACGCTG	39LREV	TCACCGTCGAGACCGTTGTCG
11AFOR	CCATGCAGTACAAGCTGATTCTGAACGCTAAAGCCGAAAGG	40GREV	CGCTCGTGTAGGTCATTCAACCGCCGACACCGT
9A_11AFOR	CCATGCAGTACAAGCTGATTCTGAACGCTAAAGCCGCTG	41EREV	CGTCGTGTAGGTCATTCCCTCGTGCACACC
24EFOR	CGAAGCTGTAGACGCTGAGACTGCAAGAGAAGG	40G_41EREV	CGCTCGTGTAGGTCATTCCCTCGGCCGACACC
24EREV	CCTCTCTGCACTCAGCGTCTACAGCTTCG	39L_40GFOR	GCTAACGACAACGGTCTGGCGGTGA
34MFOR	GCAGTACATGAACGACAACGGTGTGACG	39L_40GREV	CGAGACCGTTGTCGTTAGC
34MREV	ACCGTTGTCGTTATGACTGCTTGAACACCTTC		

Table S2: dataset

The raw sequencing counts (input and selection total) are provided for all double mutants, single mutants, and wild type in a separate excel file. We also provided single mutant fitness values together with double mutant raw counts to facilitate calculations of epistasis. Additional calculations can be performed according to the methods described here or as per alternative models.

Table S3: affinity validation

Mutant	$\Delta \ln(K_A)$ screen	$\Delta \ln(K_A)$ literature	Reference
T25A	0.17±0.01	-0.41	[S30]
K28A	-3.12±0.03	-2.12	[S30]
K31A	-5.88±0.02	-5.87	[S30]
N35A	-4.50±0.02	-3.99	[S30]
D40A	0.89±0.04	-0.46	[S30]
E42A	0.51±0.07	-0.65	[S30]
W43A	-5.72±0.12	-6.39	[S30]
T44A/Y45A	-3.35±0.15	-3.30	[S30]
W43F	-4.47±0.12	-5.67	[S31]
GB2*	1.78±0.33	1.95	[S32]
E27A [#]	-6.21±0.14	<-8.28	[S30]

* $\Delta \ln(K_{A,GB2})$ -screen was estimated by summing each of the six single mutant $\Delta \ln(K_A)$ and each of the 15 pairwise epistasis values.

[#]The lethal E27A mutant was not included in the linear regression (Figure 2A) as the reported affinity is too low to quantify by experimental means and is also below the detection limit of our screen.

Table S4: Published and predicted change in free energy of unfolding. Related to Figure 5.

Mutant	$\Delta\Delta G_U$ (kcal mol ⁻¹)*	$\Delta\Delta G_U$ screen**	W	Reference
N37L	1.43	0.64	0.31±0.02	[S33]
T16I	1.34	0.81	0.84±0.02	[S27]
T16L	1.08	0.58	0.76±0.01	[S33]
T18I	0.76	0.22	0.86±0.02	[S33]
V21P	0.50	0.43	0.92±0.01	[S26]
D47A	0.49	0.04	1.71±0.14	[S25]
T25E	0.48	0.03	0.35±0.01	[S27]
V29F	0.41	0.43	1.00±0.03	[S27]
E15V	0.38	0.11	1.49±0.04	[S33]
T18L	0.33	-0.09	0.59±0.01	[S27]
T25A	0.22	0.26	1.16±0.01	[S25]
T53Y	0.06	-0.36	0.59±0.02	[S6, S28]
T53I	-0.11	-0.62	0.76±0.02	[S6, S28]
T44S	-0.20	-0.26	1.17±0.04	[S34]
K10P	-0.20	-1.34	0.40±0.02	[S26]
T53F	-0.26	-0.71	0.54±0.02	[S6, S28]
A23P	-0.30	-0.53	1.08±0.02	[S26]
A24V	-0.33	-0.45	1.63±0.04	[S21]
T53V	-0.35	-0.65	1.07±0.04	[S6, S28]
T16A	-0.38	-0.61	0.44±0.02	[S25]
A24T	-0.38	-0.38	2.43±0.10	[S34]
T53M	-0.42	-0.61	0.80±0.03	[S6, S28]
T53W	-0.44	-0.54	1.01±0.04	[S6, S28]
T53S	-0.45	-1.09	1.17±0.04	[S6, S28]
T18A	-0.46	-0.73	1.11±0.03	[S25]
E15A	-0.47	-0.57	0.90±0.02	[S25]
A24S	-0.48	-0.40	2.09±0.07	[S34]
A24P	-0.50	-0.18	3.47±0.22	[S26]
T44E	-0.52	-0.47	0.99±0.03	[S34]
V29K	-0.53	-0.40	2.27±0.12	[S27]
A24R	-0.55	-0.56	0.47±0.01	[S34]
T53C	-0.58	-0.89	0.92±0.01	[S6, S28]
T11A	-0.60	-0.47	0.35±0.02	[S25]
T44V	-0.66	-0.62	0.49±0.01	[S34]
T44F	-0.67	-0.60	1.02±0.03	[S34]
V29A	-0.70	-0.56	1.34±0.05	[S25]
A48P	-0.70	-0.98	1.27±0.06	[S26]
T49A	-0.72	-1.03	1.18±0.06	[S25]
T44Y	-0.72	-0.58	0.87±0.03	[S34]
T44C	-0.75	-0.87	0.96±0.03	[S34]
T53L	-0.75	-1.35	0.56±0.004	[S6, S28]
I6R	-0.76	-0.95	1.10±0.12	[S22]
T44Q	-0.79	-0.54	1.44±0.05	[S34]
T53R	-0.81	-1.23	0.90±0.02	[S6, S28]
T44I	-0.81	-0.85	0.58±0.02	[S34]
T44A	-0.83	-0.61	1.46±0.06	[S34]
T44H	-0.84	-0.31	1.13±0.04	[S34]
T44M	-0.85	-0.72	1.17±0.05	[S34]
T53K	-0.92	-1.35	0.95±0.03	[S6, S28]
T53Q	-0.93	-1.32	1.02±0.03	[S6, S28]
T44D	-0.93	-0.73	0.69±0.02	[S34]
Q32G	-1.00	-1.17	1.50±0.01	[S25]
T44W	-1.00	-0.93	1.27±0.04	[S34]
T53N	-1.01	-1.67	0.76±0.03	[S6, S28]
T53H	-1.06	-1.34	0.68±0.02	[S6, S28]
T44L	-1.07	-0.87	1.01±0.04	[S34]
T44N	-1.07	-0.87	0.83±0.03	[S34]
T53E	-1.11	-1.64	0.96±0.03	[S6, S28]
I6L	-1.16	-1.01	1.42±0.13	[S35]
T44K	-1.23	-0.74	1.23±0.03	[S34]
T44R	-1.26	-0.89	1.22±0.04	[S34]
D22G	-1.40	-2.11	1.48±0.01	[S36]
F30L	-1.42	-1.71	0.79±0.02	[S25]
T53A	-1.46	-1.59	1.00±0.03	[S6, S25, S28]
I6N	-1.53	-1.88	0.84±0.10	[S23]
I6T	-1.60	-1.88	1.08±0.12	[S23]
Y3L	-1.62	-2.72	0.79±0.07	[S25]

T44G	-1.68	-1.24	1.40±0.04	[S34]
D46A	-1.74	-2.12	1.23±0.05	[S25]
D22A	-1.75	-2.22	1.66±0.01	[S25]
L7A	-1.85	-2.37	0.93±0.004	[S25]
T51A	-1.87	-2.11	0.84±0.03	[S25]
I6A	-2.09	-1.91	0.74±0.08	[S25]
T53D	-2.13	-2.07	0.63±0.01	[S6, S28]
A20G	-2.39	-1.76	0.92±0.01	[S25]
G9P	-2.40	-2.19	0.24±0.01	[S26]
T53G	-2.44	-2.50	1.78±0.10	[S6, S28]
A34G	-2.48	-1.96	0.25±0.01	[S25]
T25P	-2.80	-2.66	1.20±0.01	[S26]
V54A	-2.93	-2.54	1.18±0.05	[S25]
A26G	-2.96	-2.57	1.15±0.01	[S25]
Y45L	-3.34	-2.25	0.44±0.01	[S25]

*Published value. Average when more than one reference available.

**Predicted by screen. Average value from five reference backgrounds

Table S5: Prediction of multiple mutant stability. Related to Figure S3.

Mutant	$\Delta\Delta G_u$ (kcal mol ⁻¹)	$\Sigma\Delta\Delta G_u$	$\Delta\Delta G_{u,1}^*$	$\Delta\Delta G_{u,2}^*$	$\Delta\Delta G_{u,3}^*$	$\Delta\Delta G_{u,4}^*$	$\Delta\Delta G_{u,5}^*$	$\Delta\Delta G_{u,6}^*$	$\Delta\Delta G_{u,7}^*$	Reference
Gβ1-c3 (Y3F/L7I/V39I)	0.5	0.53	-0.05	0.58	0.00					[S20]
V21P/A23P	-0.1	-0.10	0.43	-0.53						[S26]
GB2 (I6V/L7I/E19K/A24E/V29A/E42V)	-1.0	-0.28	-0.34	0.58	-0.44	0.22	-0.56	0.26		[S37]
I6V/T53A	-2.4	-1.92	-0.34	-1.59						[S34]
L5V/I6V/L7F/V54L	-2.8	-3.01	-2.26	-0.34	-0.26	-0.67				[S35]
I6V/L7V/F52L	-3.8	-2.60	-0.34	-0.21	-2.06					[S35]
Gβ1-c3b4 (Y3F/L7I/V39I/T16I/T18I/T25E/V29I)	4.3	1.85	-0.05	0.58	0.00	0.81	0.22	-0.04	0.32	[S20]
M2 (E15V/T16I/T18I/N37L)	6.8	1.79	0.11	0.81	0.22	0.64				[S21]

*Predicted by screen. Average value from five reference backgrounds

SUPPLEMENTAL EXPERIMENTAL PROCEDURES

Library construction.

The template DNA encoding GB1 includes a T7 promoter and 5'UTR, as well as a constant 3' linker sequence encoding a Flag-tag for affinity purification from the *in vitro* translation reaction (see Figure S1C). Our template includes the sequence variation T2Q in order to minimize N-terminal heterogeneity (Smith et al., 1994) Primers with degenerate bases were used to randomize individual codons covering all possible amino acid substitutions (NNK or NNS). See Table S1 for all oligonucleotide sequences. The randomization scheme was chosen in order to eliminate the possibility of BciVI recognition sequences occurring in the coding region. Unique bases were chosen at the third codon position to distinguish the mutated position from sequencing error (Figure 1A). To assemble the library, first, adjacent random cassettes were created by PCR amplification of the template with the T7 forward primer and mutagenic reverse primers for cassettes 1-10 separately to generate ten 5' fragments (KOD polymerase from EMD). The 3' fragments were PCR amplified with mutagenic forward primers and the Flag-tag reverse primer for cassettes 2-11. Constant primers flanking the cassette (corresponding to the restriction recognition sequence and adjacent non-coding sequence) were used to make fully complemented cassettes by sub-saturation PCR as mutagenic primers produce mismatched segments that may ligate inefficiently. The cassettes were digested with BciVI (NEB), ligated to the corresponding adjacent cassette, and gel purified (see Figure S1B for an example). Using a single base overhang enabled specific ligation with a degenerate scheme (K/M) to cover all possible amino acid substitutions when the final codon of each cassette was randomized. The 5' double mutant cassette 1 was ligated to the constant 3' cassette and 3' double mutant cassettes 2-11 were ligated to corresponding constant 5' cassettes. The 5' single mutant cassette fragments 1-9 were also individually ligated to constant 3' fragments, pooled and PCR amplified for ligation to individual mutagenic 3' cassettes 3-11. For example, full-length templates with random regions 1-5 were amplified together using constant reverse primer 6, digested, and ligated to 3' random cassette 7. Finally, all full-length double mutant templates were pooled at ratios according to relative complexities. The pool encodes 536,085 double mutants, 1045 single mutants, and the wild type sequence totaling a complexity of 537,131.

mRNA Display. The library DNA template was transcribed by T7 run-off transcription (Ambion), and 1 nmole of mRNA was ligated to the pF30P linker (1.2 nmoles) via the splint oligonucleotide (1.1 nmoles) by T4 DNA ligase (NEB) in a 100 μ l reaction. After purification by urea PAGE, the mRNA template (40 pmoles) was translated using reticulocyte lysate (Ambion) in a 100 μ l reaction volume followed by incubation with KCl (500 mM final) and MgCl₂ (60 mM final) for 30 minutes at room temperature to enhance fusion formation [S38]. The mRNA-protein fusions were then affinity-purified using M2 anti-

Flag beads (Sigma-Aldrich) to remove non-fused template and sequences containing nonsense mutations. After elution with 3XFlag peptide, the fusions were reverse transcribed with super script II (Invitrogen) and a fraction of the purified sample was reserved for determination of input frequencies. Approximately 6 µg of biotinylated IgG-FC (Rockland) was bound to 15 µl of streptavidin agarose (SA) beads (Pierce) which was then divided equally to perform the affinity enrichment in triplicate. A no-target streptavidin agarose bead control was also prepared. The purified fusion sample was divided equally among the 3 IgG-FC SA bead samples and the no target control SA beads and incubated for 1.5 hours at room temperature. After washing, the immobilized fusion samples were eluted by heat (95 °C) and PCR amplified using primers to generate BciVI recognition sequences (see Figure S1C). The digested DNA was ligated to Illumina adapters created using primers listed in Table S1. In line adapter barcodes distinguished input, selected, and control pools.

Sequencing. The adapter-ligated pools were sequenced on an Illumina HiSeq (UCLA Pathology CMC core facility). The random region (165 bp) was fully sequenced by partially overlapping 100 base paired end reads. Our low complexity, single amplicon pools were mixed with non-associated high complexity pools to facilitate base calling. BWA [S39] was used to map all paired-end reads to reference sequences, which consisted of all possible single or double mutants with unique internal barcodes (Figure 1A, Table S1) in addition to wt (library- and template-derived). The mapping processes tolerated up to three mismatches to account for sequencing errors prior to error removal by barcode identification. The mapping process enabled classification of number and position of substitutions in the mutagenized cassette regions. Sequences identified with more than two random cassettes were discarded and sequences with more than two mutations within random cassettes were discarded. From the equivalent of ~4 flow cell lanes, 609,271,982 accepted sequences were obtained. A similar amount of input and combined selected pool sequences were obtained (323,082,194 and 259,540,723 respectively) while a smaller fraction of the no-target control was analyzed (26,649,065). All data processing was performed using custom python scripts (available upon request).

Data analysis. The raw data is provided in Table S2 as an excel spreadsheet. The mean input count for double mutants was 540 and the median was 248. The mean input count for single mutants was 32,283 and the median was 23,994. Variant frequencies were calculated enabling determination of binding fitness (W) by $W=(n_{mut,sel}/n_{wt,sel})/(n_{mut,in}/n_{wt,in})$. W_a' was calculated by $W_a'=(n_{ab,sel}/n_{b,sel})/(n_{ab,in}/n_{b,in})$ or $W_a'=W_{ab}/W_b$.

The triplicated selection experiment enabled determination of error for single and double mutant W when sampling was sufficient. As each of the three affinity enrichments used the same library preparation and target-bead preparation, we also summed the occurrences of all double mutants in the selected pools to derive W with higher statistical confidence. A 90% confidence interval was generated

for the fitness of double mutants by using a Poisson distribution (λ = sequencing read count) with tail probability = $22.4\% \times 22.4\% = 0.05\%$. The confidence interval for W was then estimated by $W_{CI,low}=(n_{mut,sel-Cl,low}/n_{wt,sel})/(n_{mut,in-Cl,high}/n_{wt,in})$ and $W_{CI-high}=(n_{mut,sel-Cl,high}/n_{wt,sel})/(n_{mut,in-Cl,low}/n_{wt,in})$. High confidence in observed fitness refers to $W_{high}-W_{low}\leq 0.1$ or $\ln(W_{high})-\ln(W_{low})\leq 0.5$.

By using purified fusion cDNA as the input, the screen measures fitness resulting from binding efficiency only and is not affected by differing levels of expression. Lack of solubility does not affect fitness determination as demonstrated by the lethality of sequences known to be unfolded and also the lack of binding to SA beads alone (see Figure 1B). The -IgG control enabled verification that non-specific binding did not affect determination of variant binding fitness and epistasis. As measured by pull-down assays, wt and variant fraction carryover on beads without target is less than 0.001. Given our target wt fraction bound of 0.1 a conservative estimate of the contribution to W from background binding was generated by $W_{-IgG}=0.01\times(n_{mut,-IgG}/n_{wt,-IgG})/(n_{mut,in}/n_{wt,in})$ (Figure 1B).

For epistasis calculations the sum $\ln(W_a)+\ln(W_b)$ was limited to $\geq\ln(0.01)$ to minimize spurious epistasis values for lethal or nearly lethal double mutants resulting from non-meaningful predicted fitness below the background. Also, mutational combinations that include at least one lethal mutation were capped so that $\varepsilon\geq 0$ since $\ln(<0.01)+\ln(W_b)$ cannot be predicted. Standard deviations (σ) from the triplicated experiment were used to determine error in ε by $\pm(\sigma_{Ab}^2+\sigma_{aB}^2+\sigma_{AB}^2)^{(\frac{1}{2})}$ as described [S40]. We also estimated noise in ε by using the high and low values for W_{AB} from the Poisson-based confidence interval (see above). This interval was used to minimize $|\varepsilon|$ which generated conservative estimates and eliminated spurious examples from very low fitness double mutants. For comparison to the product model (Figure S3) we did not use a confidence interval minimized value because variants with both observed and expected low fitness do not produce large epistasis values as can the relative model.

To determine relative binding affinity we used the relationship between fraction bound (F_b) and K_D , $F_B/F_{max}=[IgG]/(K_D+[IgG])$. W is related to fraction bound in the affinity enrichment by $W=F_{B,mut}/F_{B,wt}$ (see Figure S1D). Therefore $K_{D,mut}=[IgG](F_{max}/(F_{B,wt}\times W)-1)$. An approximation of $F_{max}/F_{B,wt}=8$ based on pull-down data agrees with observed maximum values of W (<8 for statistically significant double mutants). Therefore $K_{D,wt}/K_{D,mut}=7/(8/W-1)$. This estimate of binding affinity facilitated validation and enabled comparison of epistasis to energetic coupling between residues by

$$-1RT^{-1}\times\Delta\Delta G_{INT}=\Delta\ln(K_{A,ab})-\Delta\ln(K_{A,a})-\Delta\ln(K_{A,b}).$$

Validation. Thirteen single or double mutants were created by PCR using the oligonucleotides listed in Table S1. All variants constructed and characterized are described and were chosen to represent beneficial and deleterious mutations including surface and core residues near and far from the binding surface. The

variants were translated *in vitro* and assayed for binding efficiency as described previously [S41]. Briefly, mRNA templates generated by T7 runoff transcription were translated with rabbit reticulocyte rich lysate in the presence of ^{35}S -labeled Methionine. After M2 anti-flag purification labeled protein was bound to IgG labeled agarose beads for 1.5 hours at room temp. Input activity and bound activity was measured by scintillation counting. Because the *in vitro* pull down experiments generated variations in wt fraction bound from experiment to experiment due to small changes in IgG concentration the *in vitro* translated protein pull-down data was converted to ΔK_A by estimating $F_{\max}=0.7$ and therefore $\ln(\Delta K_A \text{ pull-down})=\ln(0.7/F_{B,wt}-1)-\ln(0.7/F_{B,mut}-1)$.

SUPPLEMENTAL REFERENCES

- S1. Jonsson, H., and Muller, H.P. (1994). The type-III Fc receptor from *Streptococcus dysgalactiae* is also an alpha 2-macroglobulin receptor. European journal of biochemistry / FEBS 220, 819-826.
- S2. Jonsson, H., Frykberg, L., Rantamaki, L., and Guss, B. (1994). MAG, a novel plasma protein receptor from *Streptococcus dysgalactiae*. Gene 143, 85-89.
- S3. Jonsson, H., Lindmark, H., and Guss, B. (1995). A protein G-related cell surface protein in *Streptococcus zooepidemicus*. Infection and immunity 63, 2968-2975.
- S4. Fahnestock, S.R., Alexander, P., Nagle, J., and Filpula, D. (1986). Gene for an immunoglobulin-binding protein from a group G streptococcus. Journal of bacteriology 167, 870-880.
- S5. Guss, B., Eliasson, M., Olsson, A., Uhlen, M., Frej, A.K., Jornvall, H., Flock, J.I., and Lindberg, M. (1986). Structure of the IgG-binding regions of streptococcal protein G. The EMBO journal 5, 1567-1575.
- S6. Smith, C.K., Withka, J.M., and Regan, L. (1994). A thermodynamic scale for the beta-sheet forming tendencies of the amino acids. Biochemistry 33, 5510-5517.
- S7. Olsson, A., Eliasson, M., Guss, B., Nilsson, B., Hellman, U., Lindberg, M., and Uhlen, M. (1987). Structure and evolution of the repetitive gene encoding streptococcal protein G. European journal of biochemistry / FEBS 168, 319-324.
- S8. Eyre-Walker, A., and Keightley, P.D. (2007). The distribution of fitness effects of new mutations. Nature reviews. Genetics 8, 610-618.
- S9. Roscoe, B.P., Thayer, K.M., Zeldovich, K.B., Fushman, D., and Bolon, D.N. (2013). Analyses of the effects of all ubiquitin point mutants on yeast growth rate. Journal of molecular biology 425, 1363-1377.
- S10. Firnberg, E., Labonte, J.W., Gray, J.J., and Ostermeier, M. (2014). A comprehensive, high-resolution map of a gene's fitness landscape. Molecular biology and evolution 31, 1581-1592.

- S11. McLaughlin, R.N., Jr., Poelwijk, F.J., Raman, A., Gosal, W.S., and Ranganathan, R. (2012). The spatial architecture of protein function and adaptation. *Nature* *491*, 138-142.
- S12. Khan, A.I., Dinh, D.M., Schneider, D., Lenski, R.E., and Cooper, T.F. (2011). Negative epistasis between beneficial mutations in an evolving bacterial population. *Science* *332*, 1193-1196.
- S13. Araya, C.L., Fowler, D.M., Chen, W., Muniez, I., Kelly, J.W., and Fields, S. (2012). A fundamental protein property, thermodynamic stability, revealed solely from large-scale measurements of protein function. *Proceedings of the National Academy of Sciences of the United States of America* *109*, 16858-16863.
- S14. Mani, R., St Onge, R.P., Hartman, J.L.t., Giaever, G., and Roth, F.P. (2008). Defining genetic interaction. *Proceedings of the National Academy of Sciences of the United States of America* *105*, 3461-3466.
- S15. Sauer-Eriksson, A.E., Kleywegt, G.J., Uhlen, M., and Jones, T.A. (1995). Crystal structure of the C2 fragment of streptococcal protein G in complex with the Fc domain of human IgG. *Structure* *3*, 265-278.
- S16. Tokuriki, N., Stricher, F., Schymkowitz, J., Serrano, L., and Tawfik, D.S. (2007). The stability effects of protein mutations appear to be universally distributed. *Journal of molecular biology* *369*, 1318-1332.
- S17. Aurora, R., and Rose, G.D. (1998). Helix capping. *Protein science : a publication of the Protein Society* *7*, 21-38.
- S18. Kortemme, T., and Creighton, T.E. (1995). Ionisation of cysteine residues at the termini of model alpha-helical peptides. Relevance to unusual thiol pKa values in proteins of the thioredoxin family. *Journal of molecular biology* *253*, 799-812.
- S19. Doig, A.J., and Baldwin, R.L. (1995). N- and C-capping preferences for all 20 amino acids in alpha-helical peptides. *Protein science : a publication of the Protein Society* *4*, 1325-1336.
- S20. Malakauskas, S.M., and Mayo, S.L. (1998). Design, structure and stability of a hyperthermophilic protein variant. *Nature structural biology* *5*, 470-475.
- S21. Wunderlich, M., and Schmid, F.X. (2006). In vitro evolution of a hyperstable Gbeta1 variant. *Journal of molecular biology* *363*, 545-557.
- S22. Lassila, K.S., Datta, D., and Mayo, S.L. (2002). Evaluation of the energetic contribution of an ionic network to beta-sheet stability. *Protein science : a publication of the Protein Society* *11*, 688-690.
- S23. Merkel, J.S., Sturtevant, J.M., and Regan, L. (1999). Sidechain interactions in parallel beta sheets: the energetics of cross-strand pairings. *Structure* *7*, 1333-1343.
- S24. Smith, C.K., and Regan, L. (1995). Guidelines for protein design: the energetics of beta sheet side chain interactions. *Science* *270*, 980-982.
- S25. McCallister, E.L., Alm, E., and Baker, D. (2000). Critical role of beta-hairpin formation in protein G folding. *Nature structural biology* *7*, 669-673.
- S26. Choi, E.J., and Mayo, S.L. (2006). Generation and analysis of proline mutants in protein G. *Protein engineering, design & selection : PEDS* *19*, 285-289.
- S27. Wunderlich, M., Max, K.E., Roske, Y., Mueller, U., Heinemann, U., and Schmid, F.X. (2007). Optimization of the gbeta1 domain by computational design and by in vitro evolution: structural and energetic basis of stabilization. *Journal of molecular biology* *373*, 775-784.

- S28. Minor, D.L., Jr., and Kim, P.S. (1994). Measurement of the beta-sheet-forming propensities of amino acids. *Nature* *367*, 660-663.
- S29. Potapov, V., Cohen, M., and Schreiber, G. (2009). Assessing computational methods for predicting protein stability upon mutation: good on average but not in the details. *Protein engineering, design & selection : PEDS* *22*, 553-560.
- S30. Sloan, D.J., and Hellinga, H.W. (1999). Dissection of the protein G B1 domain binding site for human IgG Fc fragment. *Protein science : a publication of the Protein Society* *8*, 1643-1648.
- S31. Walker, K.N., Bottomley, S.P., Popplewell, A.G., Sutton, B.J., and Gore, M.G. (1995). Equilibrium and pre-equilibrium fluorescence spectroscopic studies of the binding of a single-immunoglobulin-binding domain derived from protein G to the Fc fragment from human IgG1. *The Biochemical journal* *310* (*Pt 1*), 177-184.
- S32. Gronenborn, A.M., Filpula, D.R., Essig, N.Z., Achari, A., Whitlow, M., Wingfield, P.T., and Clore, G.M. (1991). A novel, highly stable fold of the immunoglobulin binding domain of streptococcal protein G. *Science* *253*, 657-661.
- S33. Thoms, S., Max, K.E., Wunderlich, M., Jacso, T., Lilie, H., Reif, B., Heinemann, U., and Schmid, F.X. (2009). Dimer formation of a stabilized Gbeta1 variant: a structural and energetic analysis. *Journal of molecular biology* *391*, 918-932.
- S34. Minor, D.L., Jr., and Kim, P.S. (1994). Context is a major determinant of beta-sheet propensity. *Nature* *371*, 264-267.
- S35. Gronenborn, A.M., Frank, M.K., and Clore, G.M. (1996). Core mutants of the immunoglobulin binding domain of streptococcal protein G: stability and structural integrity. *FEBS letters* *398*, 312-316.
- S36. O'Neil, K.T., Hoess, R.H., Raleigh, D.P., and DeGrado, W.F. (1995). Thermodynamic genetics of the folding of the B1 immunoglobulin-binding domain from streptococcal protein G. *Proteins* *21*, 11-21.
- S37. Orban, J., Alexander, P., Bryan, P., and Khare, D. (1995). Assessment of stability differences in the protein G B1 and B2 domains from hydrogen-deuterium exchange: comparison with calorimetric data. *Biochemistry* *34*, 15291-15300.
- S38. Liu, R., Barrick, J.E., Szostak, J.W., and Roberts, R.W. (2000). Optimized synthesis of RNA-protein fusions for in vitro protein selection. *Methods in enzymology* *318*, 268-293.
- S39. Li, H., and Durbin, R. (2009). Fast and accurate short read alignment with Burrows-Wheeler transform. *Bioinformatics* *25*, 1754-1760.
- S40. Chen, J., and Stites, W.E. (2001). Energetics of side chain packing in staphylococcal nuclease assessed by systematic double mutant cycles. *Biochemistry* *40*, 14004-14011.
- S41. Liao, H.I., Olson, C.A., Hwang, S., Deng, H., Wong, E., Baric, R.S., Roberts, R.W., and Sun, R. (2009). mRNA display design of fibronectin-based intrabodies that detect and inhibit severe acute respiratory syndrome coronavirus nucleocapsid protein. *The Journal of biological chemistry* *284*, 17512-17520.